POLISH
ACADEMY
OF SCIENCES
INSTITUTE
OF FUNDAMENTAL
TECHNOLOGICAL
RESEARCH

ECOLE
NATIONALE
D'INGENIEURS
DE METZ (ENIM)

ENGINEERING TRANSACTIONS

ROZPRAWY INŻYNIERSKIE - TRAITE d'INGENIERIE

QUARTERLY
VOLUME 59
ISSUE 2

WARSZAWA - METZ 2011

SUBSCRIPTIONS

Address of the Editorial Office: Engineering Transactions
Institute of Fundamental Technological Research
Pawińskiego 5B, PL 02-106 Warsaw, Poland
Tel.: (48-22) 826 60 22, Fax: (48-22) 826 98 15, E-mail: publikac@ippt.gov.pl

Subscription orders for all journals edited by IPPT (Institute of Fundamental Technical Research) may be sent directly to the Publisher: Institute of Fundamental Technological Research
e-mail: subscribe@ippt.gov.pl

Please transfer the subscription fee to our bank account: Payee: IPPT PAN,
Bank: Pekao S.A. IV O/Warszawa,
Account number 05124010531111000004426875.

All journals edited by IPPT are available also through:

- Foreign Trade Enterprise ARS POLONA ul. Obrońców 25,
  03-933 Warszawa, Poland, Tel. (48-22) 509 86 38, 509 86 37
  e-mail: arspolona@arspolona.com.pl
- RUCH S.A. ul. Jana Kazimierza 31/33,
  01-248 Warszawa, Poland,
  Tel. (48-22) 532 88 16, Fax (48-22) 532 87 31
  e-mail: prenumerata@okdp.ruch.com.pl
- International Publishing Service Sp. z o.o. ul. Noakowskiego 10 lok. 38
  00-664 Warszawa, Poland, Tel./fax: (48-22) 625 16 53, 625 49 55
  e-mail: books@ips.com.pl

Warunki prenumeraty

Prenumeratę na wszystkie czasopisma wydawane przez IPPT PAN przyjmuje Dział Wydawnictw IPPT. Bieżące numery można nabywać, a także zaprenumerować roczne wydanie Engineering Transactions, bezpośrednio w IPPT PAN,
ul. Pawińskiego 5B, 02-106 Warszawa
Tel.: (48-22) 826 60 22; Fax: (48-22) 826 98 15
e-mail: subscribe@ippt.gov.pl

Wpłaty na prenumeratę przyjmują także regionalne Działy Sprzedaży Prasy RUCH S.A. Infolinia: 804 200 600. Zamówienia można przesyłać pocztą elektroniczną ze strony www.prenumerata.ruch.com.pl

Arkuszy wydawniczych 5.75; Arkuszy drukarskich 4.50
Papier offset. kl. III 70 g. B1
Skład w systemie LaTeX K. Jezierska
Druk i oprawa: Drukarnia Braci Grodzickich, Piaseczno ul. Geodetów 47A

ENGINEERING TRANSACTIONS • *Engng. Trans.* • **59**, 2, 67–84, 2011
Polish Academy of Sciences • Institute of Fundamental Technological Research (IPPT PAN)
National Engineering School of Metz (ENIM)

CORRELATION BETWEEN DYNAMIC MATERIAL BEHAVIOR AND ADIABATIC SHEAR PHENOMENON FOR QUENCHED AND TEMPERED STEELS

F. P u r s c h e, L.W. M e y e r

Nordmetall GmbH
Hauptstrasse 16, D-09221 Adorf / Erzg., Gmd. Neukirchen

Besides the common failure mechanism based on crack propagation, adiabatic shear failure results from a collapse mechanism, mainly at high deformation rates. This failure incorporates locally extreme high shear strains, but due to the small volume involved, it transpires in a macroscopic brittle manner. This paper deals with the description of the influence of material properties on adiabatic shear failure. In the literature, much information can be found, which supports the theory that some material properties influence the occurrence of adiabatic shear failure behavior in a positive or negative manner. The determination of propensity for the investigated steels was done through special biaxial dynamic compression-shear-test in a drop weight tower. The failure achieved in the test is only material-dependent. Furthermore, it was found, that the theory of Culver with the competing processes of work hardening and thermal softening is transferable on the tested materials in a qualitative manner. Additionally, it was determined that few material properties have a strong controlling effect on the adiabatic shear failure behavior and it is possible to determine a critical value for transition between sheared and non sheared areas. Moreover, it could define a functional correlation of the failed materials to certain properties. As a main result, the most important material property is the dynamic compression behavior at high temperature. The stress level of the material and the characteristic in dependence of temperature is decisive. Analytical considerations using high temperature behavior patterns confirm this influence. Additionally, hardness and strength at room temperature and the pure shear capability (hat-shaped specimen) are also important for the evaluation of adiabatic failure behavior.

1. Introduction

In addition to the common failure mechanism based on crack propagation effects, another failure mechanism exists; this additional failure mechanism, which occurs mainly at high deformation rates, is the adiabatic shear failure. This localized failure yields to a macroscopic brittle rupture and thereby, to a reduction in the energy consumption. This failure behavior occurs in various technical areas, such as machining, forging, blanking, ballistics (target and penetrator), crash, surface friction, and detonative loading. The adiabatic shear failure behavior

is mainly exhibited in metallic materials, like steel, titanium or aluminium, although it can also appear at plastics, rocks or ceramics.

In the literature much information can be found which supports the theory that some material properties influence the adiabatic shear failure behavior in a positive or negative manner. Tresca [1] and Zener and Hollomon [2] have observed that the strength and the heat capacity, as well as the thermal softening of the materials, have an important influence on the adiabatic shear behavior. Nowadays it is known that a lower strain hardening coefficient [3–5], a lower strain rate dependence [6–7], a lower heat capacity or thermal conductivity [3–5], a lower grain size [3, 8] or a lower density of the material [7–9], promote the adiabatic shear failure behavior. Additionally, a high hardness [10–13], a high strength [3, 4, 14, 15], a high thermal softening [3–5], a high loading velocity [5, 8, 16], a high pre-deformation [3, 17], and a high specimen size [18], promotes the adiabatic shear failure behavior too. Furthermore, additional properties exist, for example initial temperature [19], hydrostatic stress state [20, 21], and tensile loading [4]. Even considering these factors, they may promote or inhibit adiabatic shear failure depending on the precise circumstances.

The question then arises: which material properties have the strongest influence on adiabatic shear failure for the investigated materials in this study? Observing and measuring the adiabatic shear failure behavior was accomplished through the performance of materials under different experimental tests, firstly with compression and compression-shear-loading. Furthermore, there is much discussion concerning high temperature compressive strength, the Culver-theory [22], analytical consideration and a description of the correlation between the material properties and the adiabatic failure behavior of the materials.

The aim of this study is to point out the material properties which have strong influence on the adiabatic shear failure behavior for high strength low-alloyed steels. Is it possible to find correlations and associated material properties? The next issue involves the validity of the Culver-theory on the observed materials and a discussion of the influence of high temperature behavior on the adiabatic failure process.

2. Adiabatic shear phenomena

The beginning of the adiabatic shear failure process is initiated by mutual displacement of material areas. This displacement is shown through the alignment of segregation lines in the vicinity of a transformed shear band in a certain quenched and tempered steel (Fig. 1).

This deformation process undergoes mainly of high deformation velocity and is locally concentrated. Because of the high strain rate, the generated heat due to the strain hardening cannot dissipate in the surrounding material; thus, a tem-

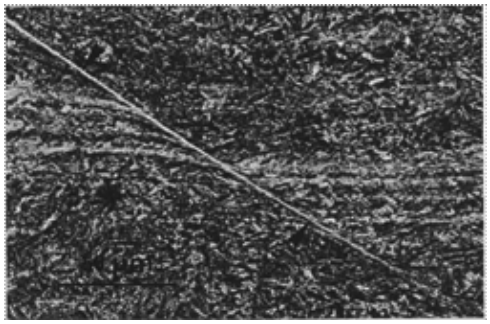

FIG. 1. Transformed shear band with segregation lines after DORMEVAL 1987.

perature rise will develop in the deformed region. Hence, a local temperature rise and a temperature gradient in the specimen, or in a component of the specimen, occur and manifest as a localized strength reduction. This process is further amplified and more localized, while further inducing a decrease in strength until the formation of an adiabatic shear band occurs and finally the failure appears.

The difference between the appearance of an adiabatic shear failure and the appearance of a classical fracture is shown in Fig. 2. In the classical fracture evaluation there is a differentiation from a brittle fracture compared to a ductile mixed and a pure ductile shear fracture. This ductile fracture is forced through shear stresses similar to the behavior under compression-shear-loading (Fig. 2 lower left). At very high loading rates, a local adiabatic deformation occurs and the rupture concentrates to low volumes, which is leading to brittle kind of fracture with low global, but high local energy consumption. The final result is comparable to the classical brittle fracture.

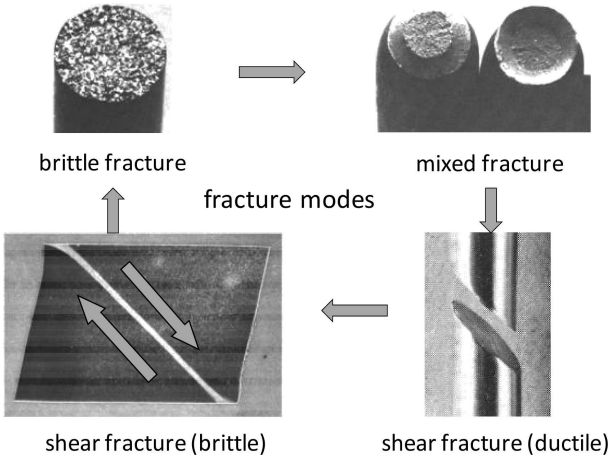

FIG. 2. Comparison of classical fracture modes to the adiabatic shear failure.

The investigations on adiabatic shear failure began in 1879 with TRESCA [1]. He described the phenomenon of forging cross on a Pt-Ir-alloy and observed that a material's strength and heat capacity have an important influence on its adiabatic shear failure. In 1944, ZENER and HOLLOMON [2] originated the theory of thermal instability due to the intense plastic deformation. Further research into the effects of strengthening and softening was conducted by RECHT [23] in 1964 and CULVER [22] in 1973. In the decades from the 1960s to the 1990s, investigations concerning the influence of the material behavior to the adiabatic shear failure were made by ROGERS [24], DORMEVAL [4], MEYERS [25], and BAI and DODD [20]. In more recent years, studies of mechanical description have been made by CLIFTON [26] and WRIGHT [27]. Additionally, studies of the microstructure of the initiation and development of shear bands have been performed by MEYERS [28] and XU [5].

Published literature contains a broad range of statements, which properties have an influence on the initiation of the adiabatic shear failure. These results can be divided into four groups. One group deals with the stress state (shear strength, shear strain, shear rate); a second group deals with the loading conditions such as temperature, stress state, energy or velocity. The third group deals with the microstructure of the material (precipitations, inclusions, voids etc.) and the fourth group describes the influence of the material properties such as density, heat capacity, strain hardening coefficient or thermal softening. The present study will be concentrated on the fourth group, material properties.

There are different assumptions for the critical condition of the beginning of the adiabatic shear failure. Most authors assume it is necessary to reach a certain amount of strain (CULVER [22], BAI and DODD [20] or STAKER [29]). Other authors contend that a certain level of strain rate is crucial for the initiation of adiabatic shear bands (RECHT [23] and KLEPACZKO [30]). WANG *et al.* [31] and XU [5] describe a critical value as a consideration for strain and strain rate. Furthermore, there are assumptions that a critical energy must exist (WANG and RITTEL [19]) or that a definite fracture toughness value are necessary (GRADY [32]). Nowadays there are results that a dynamic recrystallization (called DRX) is responsible for the initiation condition [45, 46].

A well-known theory for describing of adiabatic shear failure is based on the principle from the work hardening and thermal softening of the material. These competing processes are described in a relation that shows the parts separately (Eq. (2.1)).

$$d\sigma = \left(\frac{\partial\sigma}{\partial\varepsilon}\right)_{\dot{\varepsilon},T} d\varepsilon + \left(\frac{\partial\sigma}{\partial\dot{\varepsilon}}\right)_{\varepsilon,T} d\dot{\varepsilon} + \left(\frac{\partial\sigma}{dT}\right)_{\dot{\varepsilon},\varepsilon} dT. \tag{2.1}$$

Adiabatic shear failure can occur, when the thermal softening of the material overcomes the strengthening due to the strain hardening and the strain rate

hardening [4, 23, 25, 27]. The first term described the strain hardening, the second term – the strain rate hardening and the third term the thermal softening behavior, which acts against the first and second term. With the negligence of the second part and the differentiation with $d\varepsilon$, a criterion can be formulated for instability (Eq. (2.2); RECHT [23], CULVER [22], BAI and DODD [20]):

$$\left(\frac{\partial\sigma}{\partial\varepsilon}\right)_{\dot{\varepsilon},T} + \left(\frac{\partial\sigma}{\partial T}\right)_{\dot{\varepsilon},\varepsilon} \frac{dT}{d\varepsilon} = 0. \tag{2.2}$$

The left term describes the influence of the strain hardening and the right term – the thermal softening behavior. The failure behavior can be imagined as a form of a convex adiabatic curve. When the equilibrium of both competing processes is reached, identical with the apex of the curve, an adiabatic shear failure can occur. From the above displayed softening theory CULVER [22] has evolved a plain relation (Eq. (2.3)) to predict the failure strain of the material. Culver has made three assumptions. The strain hardening coefficient n_T from the isothermal behavior will substitute through the static one. The thermal softening behavior of the materials will remain linear and the stress relation (σ_T/σ_D) between dynamic isothermal and the dynamic adiabatic value will be neglected. Furthermore the density, the heat capacity and the Taylor-Quinney factor are contained.

$$\varepsilon_i = \frac{n_T \cdot \rho \cdot c_p}{0.9(\partial\sigma/\partial T)} \cdot \frac{\sigma_T}{\sigma_D}. \tag{2.3}$$

One objective of this study is to evaluate whether this theory from Culver is applicable to the investigated materials. The second objective of the examination, is to determine if there are additional material properties other than the thermal softening or hardness, which may influence the adiabatic shear failure behavior.

3. Test procedure and materials

Many different experimental methods exist to determine the propensity of a material to fail under adiabatic shear condition. Several test techniques are based on geometrical discontinuities, such as pure torsion [3, 4, 20, 27], hat-shaped [5, 27, 33, 40], single or double edge [16, 34], and punch loading [2, 3, 20, 43]. Alternatively, some techniques exist, where the failure is mainly dependent on the material behavior and is not initially influenced by geometry effects, such as compression [4, 27], compression-shear [35–37] or cylinder expansion test [5, 10, 20].

The determination of propensity for the investigated materials was done through a special biaxial dynamic compression-shear test at about 2 m/s in

a drop weight tower, Fig. 3. The drop weight has a mass of 600 kg and can be stopped at desired displacement; thus, a visualization of development of adiabatic shear bands versus applied strains or from dark to white etching character is possible. This compression-shear specimen was invented by MEYER and STASKEWITSCH [39, 44] so that a wider differentiation of materials is available to contrast against the plain compression loading. For this reason the usual compression specimen is inclined a few degrees against the loading axis, with the effect of an enhanced multiaxial compression/shear loading. Depending on the desired amount of additional shear stresses, the inclination can be varied to max 10°. The specimens used in this study were 6° inclined. This little inclination will induce a certain biaxial compression-shear state in the specimen. Already this stress-state with only 10% of additional shear stresses challenges the material to fail with adiabatic shearing or not.

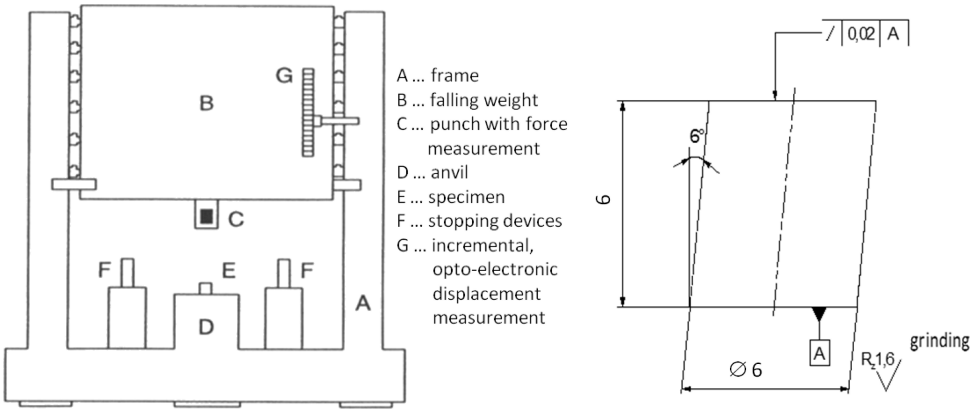

FIG. 3. Drop weight tower and test specimen.

The advantage of this technique is the absence of the influence of a stress enhancement like a surface flaw or a notch on the failure strain. The failure development is only dependent on the material's properties. As the first result of this test, it can be determined whether or not there is an occurrence of adiabatic shear failure. When shear failure occurs, a corresponding axial failure strain can be determined. Therefore, it is possible to give a qualitative and a quantitative result for an evaluation of the propensity of materials for adiabatic shear failure.

Additional tests were used for the determination of the correlations between material properties and adiabatic shear failure. Conducted were compression tests at room temperature and at high temperature, in order to measure the material's strength for the evaluation of the thermal softening of the materials. An often used technique is the use of the hat-shaped specimen, which was created by HARTMANN and MEYER [40]. The advantage of the hat-shaped test is that

it can be used to test very ductile materials in a Compression-Setup such as SHPB or drop weight tower and a comparison between small and larger failure strain can be made. Tension tests were used for static and dynamic (1 m/s) velocities with a rotating wheel to determine values of strength and ductility. Also hardness tests, Charpy impact and fracture toughness tests were performed.

The materials used were several quenched and tempered steels with a broad range of hardness between 300 and 600 HB. The microstructure of the materials is a tempered martensitic structure.

4. Experimental results and discussion

Biaxial compression-shear tests were performed to verify the propensity to adiabatic shear failure of the materials. The specimens were tested at approximately 2 m/s with a drop weight device at room temperature. During the test the force and the displacement were both measured. A representative selection from all the materials with the axial engineering or technical compressive stress versus the axial technical strain is shown in Fig. 4 (left). It can be seen that two different behaviors exist. A few steels, with lower flow stresses, exhibit a more or less homogenous deformation until the limitation of displacement is reached. The other group of materials (about half of the investigated materials), shows sudden stress drop at lower strains. At this point the material failed due to adiabatic shearing. This measured amount of reduction for all failed materials was applied to determine additional correlations. It can be seen that exist different failure strengths and failure strains for the different steels. An initial consideration of the stress level shows that high strength steels are much more prone to adiabatic shear failure than the lower strength materials. This correlates to the hardness of the materials, Fig. 4 (right). With low hardness values, no adiabatic

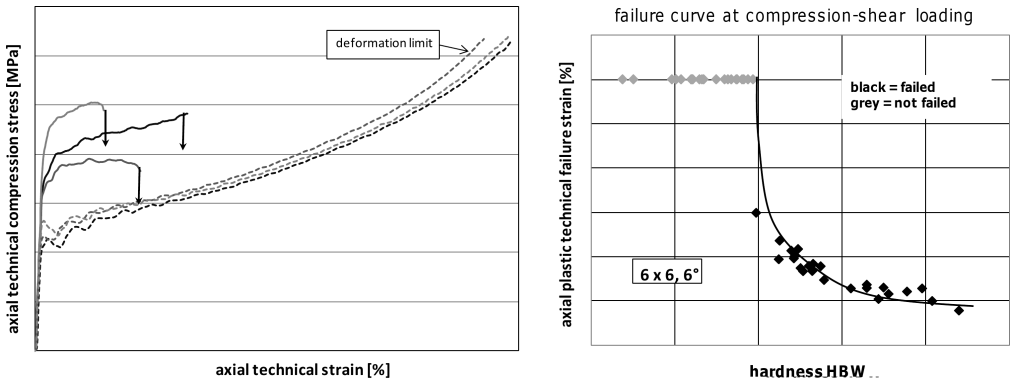

Fig. 4. Stress-strain behavior of the compression-shear test ($\dot{\varepsilon} = 200\ \mathrm{s}^{-1}$) and the correlation with the hardness.

shear failure occurred. The grey points are defined at a deformation limit of the drop weight device. At certain hardness, first times adiabatic shear failure begins. As the material's hardness increases, the failure strain declines along with potential function. These results are valid for the materials and for the strain rate of $\dot{\varepsilon} = 200\ \mathrm{s}^{-1}$ investigated in this study. This dependence, already cited in the literature, is hereby confirmed.

The next examinations involve (pure) compression loading at room temperature. A selection of true stress-true strain-diagrams of the investigated materials at a strain rate of $\dot{\varepsilon} = 200\ \mathrm{s}^{-1}$ is shown in Fig. 5. The material behavior under this adiabatic condition begins at the lowest strength level with a pure strain hardening behavior, for example of a plain carbon steel. In the medium strength level, for example HSLA-steel, there an equilibrium between strain hardening and softening is existing. At the highest strength level mainly a softening behaviour occurs. These flow stress variations, responding to the hardening or softening behavior under dynamic compression loading, are arranged after their amounts in Fig. 5 (right). It can be seen that materials with a strong decline are prone to fail through adiabatic shearing. On the other hand there is an area with positive values, i.e. a hardening behavior. These materials most likely do not fail. In the depicted middle range, no clear dependence between the decline or softening behavior and the adiabatic shear failure is found. Thus, a conclusion can be made that the plain decline behavior under adiabatic compression is not clearly correlated with the adiabatic shear failure, at least not for this particular quenchend and tempered material group. The strain hardening coefficient, even at a strain rate of 200 1/s, which shall have an important influence on the adiabatic failure behavior, as described in the literature, cannot be confirmed for this material steel group. There might be a tendency, but for most of the steels a clear relation cannot be drawn.

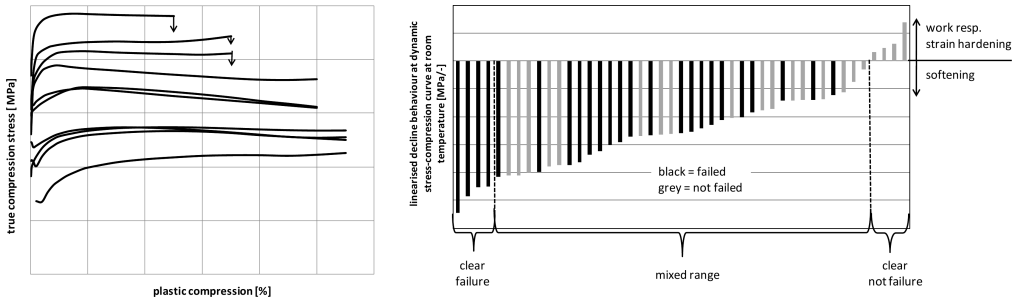

FIG. 5. True stress- true strain curves at (pure axial) dynamic compression ($\dot{\varepsilon} = 200\ \mathrm{s}^{-1}$) and results of softening determination.

The third investigation was to determine the stress behavior at high temperature under dynamic compression loading. The first result exhibits the dif-

ferent strength levels of the different steels, Fig. 6 (left). This distinct difference in flow stress lasts until about 600°C. With higher flow stress, the propensity to adiabatic shear failure is increased (arrow in Fig. 6). Materials with a high strength at room and at elevated temperatures are prone to adiabatic shearing. Furthermore, these materials show a rapid loss of strength with increased temperature. These drops of strength yield a development of a gradient of temperature-dependent stress resistance. This gradient is considerably higher for high strength steels. For low strength steels, the gradient is hardly sensible, and therefore these steels are not prone to adiabatic shearing, for example valid for the three curves depicted with no failure in Fig. 6. The results of the determined values of the linearized decline behavior at the stress-temperature-curves between temperatures of −100°C and 750°C is shown in Fig. 6 (right). There is a good correlation of the normalized strength decline value to the occurrence of adiabatic shear failure under compression shear loading. The stronger the decline behaviour, the lower the failure strain under compression-shear-loading will be. Above a certain value, no more failure occurred.

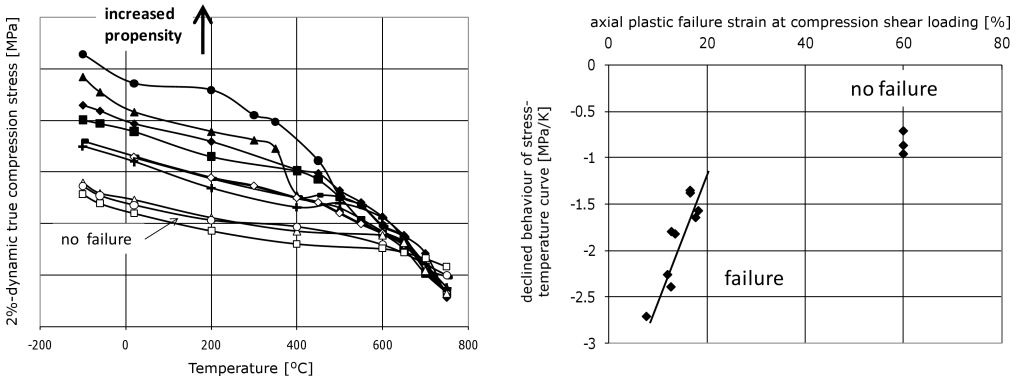

FIG. 6. Dynamic 2%-flow compression stress vs. starting temperature and determined declined flow stress values at dynamic strain rate of ($\dot{\varepsilon} = 200\ \mathrm{s}^{-1}$) between −100°C and 750°C.

The determined failure strains according to Culver (Eq. (2.3)) show a good qualitative correlation, Fig. 7. All materials with low calculated failure strain fail under compression-shear loading too. High values correlate with the materials with no failure. The depicted transition state is in the limit range of the used compression-shear loading test configuration. For the failed states, the correlation between the experimental and the calculated failure strain, Fig. 7 (right), show an absolute insufficient agreement. Thus, according to Culver for the investigated materials, it is only possible that a qualitative correlation with the softening theory exists.

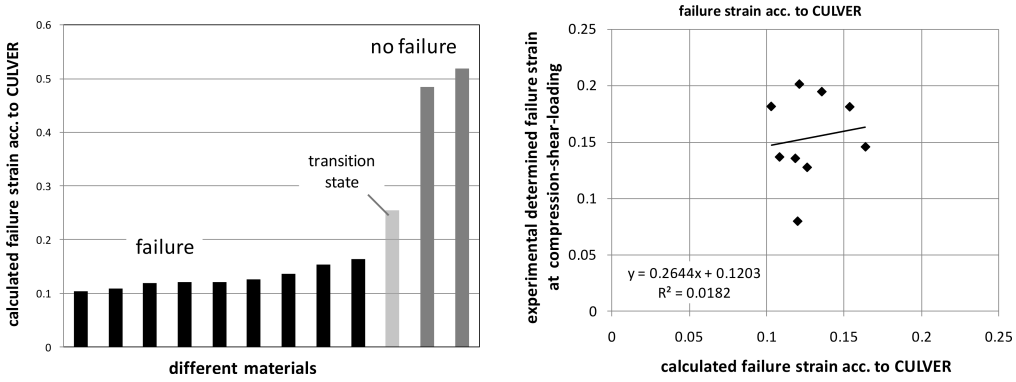

FIG. 7. Qualitative and quantitative evaluation of the materials using Culver-theory.

In addition to the previous examinations, stress-temperature-characteristics were also considered. Two examples of dynamic flow compression stress versus temperature are shown in Fig. 8. The left material shows a distinctive drop in strength; the right material shows at a certain temperature a change in the decline behavior. These points represent a change in the softening behavior from a low to high or higher decrease. These points are called "instability points" and from this, the related temperatures and stress values are obtained.

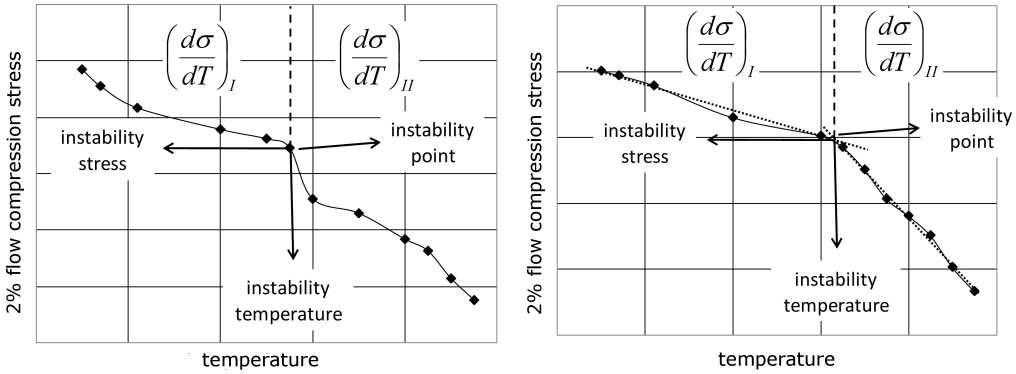

FIG. 8. Examples for determined instability points from dynamic flow compression stress vs. temperature ($\dot{\varepsilon} = 200\ \mathrm{s}^{-1}$).

The instability temperatures were correlated with the failure strain at compression-shear loading (Fig. 9, left). In the sheared area is a linear agreement with higher failure strain a higher instability temperature is determined. Above the instability temperature of 600°C there is no more failure. The determined instability temperatures and stresses for all materials were then depicted, Fig. 9 (right). With lower instability temperature and higher instability stress, the propensity to adiabatic shear failure increases. These results show that the spe-

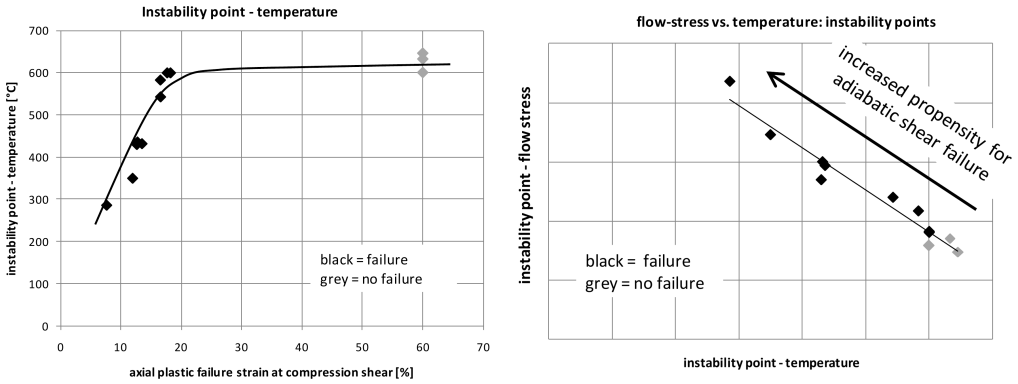

FIG. 9. Instability points of temperature versus failure strain at compression-shear loading and correlation of instability temperatures and stresses for all materials.

cific stress-temperature characteristic of the materials, especially the "instability points", from this study is a very valuable information and that the use of linearized decrease behavior is not always sufficient.

Previous results prove that the dynamic high temperature behavior of the materials is important for the evaluation of the propensity of adiabatic shear failure. The measured compression flow stress behavior at elevated temperatures was used to study the stress-strain-temperature-field analytically. The assumption (Fig. 10) is that the stress is a function of temperature, the temperature is a function of strain, and the strain is a function of a local position. Considering slow shear deformation, there is normally a homogenous distribution of strain and thus a homogenous distribution of temperature and stress. In the case of

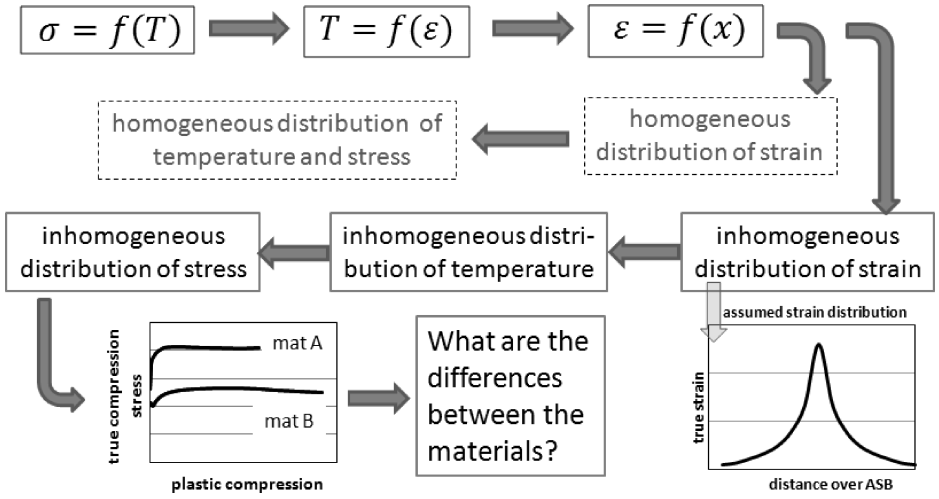

FIG. 10. Approach for the analytical consideration.

impact loading, an adiabatic deformation occurs. The related deformation field is inhomogeneous, like a strain distribution across the shear band, Fig. 10, lower right. This certain distribution yields an inhomogeneous distribution of temperature and stress (or a consequence). The used materials have different strength levels that evoke a different temperature rise in the specimen for the same deformation [41].

This different temperature behavior leads to a different stress resistance behavior, according to FENG and BASSIM [42], across the shear band, Fig. 11 (left). Material A shows a considerable loss in stress resistance and thus a development of a strong gradient. This gradient is caused by the stress-temperature-behavior, similar to these in Fig. 8. This gradient leads to a local increased deformation and therefore to a local failure. Material B shows only a small loss of stress resistance; thus, this material is not susceptible to adiabatic shear failure. For the evaluation of the propensity to adiabatic shearing, the strength level and the intensity of the gradient are both important. From the analytically calculated temperature and stress gradient behaviors for all materials across the shear band, the minimum of stress resistance and the maximum of temperature (from the apex) was used to create a correlation between the calculated inner local temperature and inner stress resistance. These determined points show a linear dependence that with an increased local temperature, the propensity to adiabatic shear failure increases, Fig. 11 (right). After analytical consideration, these results confirm the conclusion that the stress-temperature behavior is important for the evaluation of the propensity of adiabatic shearing.

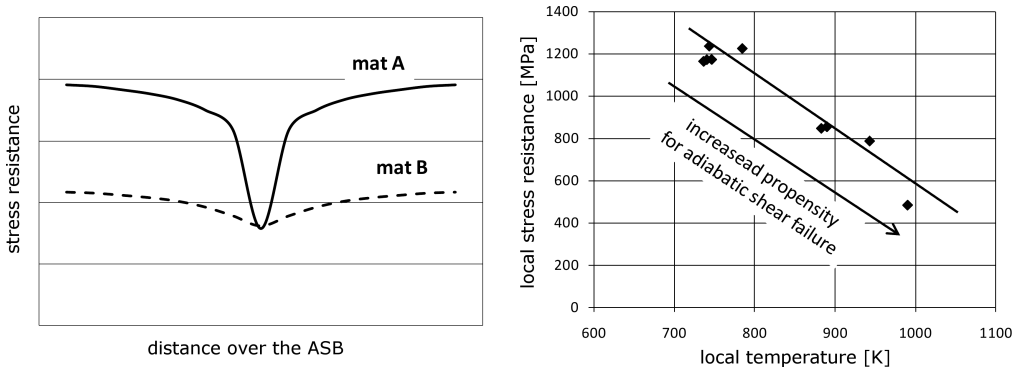

FIG. 11. Results of the analytic consideration and correlation to adiabatic shear failure.

Also interesting is the found result, that a correlation between the displacements, leading to failures, in the "hat" test and the inclined compression shear test, is existing. The failure strains at compression-shear loading correspond to the shear failure behavior at hat-shaped tests with a linear dependence, Fig. 12.

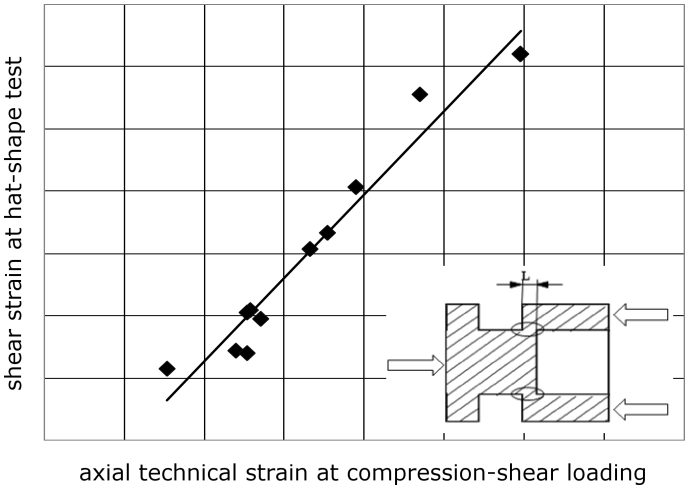

FIG. 12. Correlation of shear failure at hat-shape-test to the compression-shear failure.

This behavior is explained through the mutual influence of the mainly shear stress loading condition on the failure behavior for both test techniques.

For several material properties, a correlation to the adiabatic shear failure behavior was not found, like compression strain hardening coefficient at elevated temperatures, fracture strain and energy assumption at tensile loading, fracture toughness under mode I, and Charpy impact energy. As the reason, different loading conditions, which are not comparable and will lead to different failure modes, are assumed to be responsible.

GRADY [32] defined a shear fracture energy per unit area (Eq. (4.1)), which is necessary for initiation of shear band formation; surely, this approach is useable for the evaluation of materials for the propensity to adiabatic shear failure. In addition to Culver's theory, there are other properties involved such as thermal conductivity, flow shear stress and strain rate.

$$\Gamma = \frac{\rho \cdot c}{\alpha} \left(\frac{9 \cdot \rho^3 \cdot c^2 \cdot \chi^3}{\tau_y^3 \cdot \alpha^2 \cdot \dot{\varepsilon}} \right)^{1/4}, \tag{4.1}$$

where Γ – fracture energy per unit area, ρ – density, c – specific heat, χ – thermal conductivity, τ_y – flow shear stress, α – thermal softening, $\dot{\varepsilon}$ – strain rate.

With determined energy values (Fig. 13 left), a good differentiation to the tested materials is possible. Materials with a high amount of energy consumption correspond to the "no failure"-states and all materials with a low energy value failed under compression shear-loading. The difference between these two areas is considerable. Furthermore, in contrast to the theory of CULVER [22], there

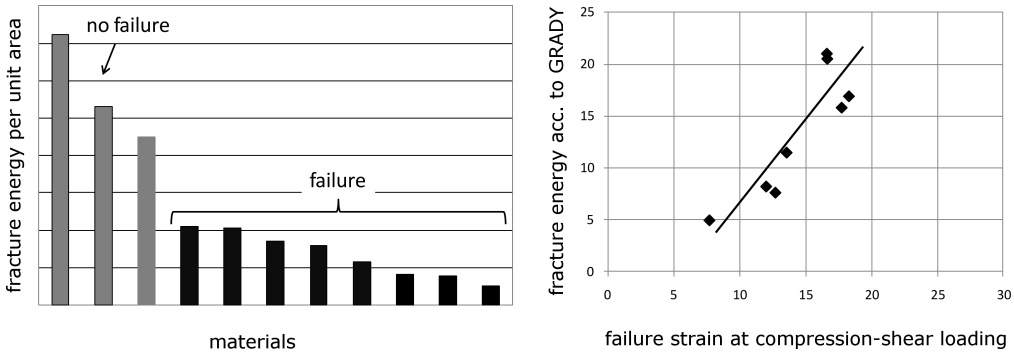

FIG. 13. Fracture energy acc. to Grady and the correlation to adiabatic compression-shear failure.

is a possibility of defining a quantitative correlation with the shear fracture energy of GRADY [32]. This fracture energy, according to Grady, corresponds in a nearly linear agreement to the energy consumption until failure occurs at dynamic compression shear loading, Fig. 13 (right).

It is possible to summarise the results to an assessment, Fig. 14, because of the properties that give a correlation to the adiabatic shear failure behavior.

Property	Qualitative consideration	Quantitative consideration	Assessment rating
	threshold value	R^2-value	
instability point of **temperature** from dynamic stress-temperature-behavior	Yes	0.95	very good
shear failure from dynamic „hat"-shape-test	Yes	0.95	
instability point of **stress** from dynamic stress-temperature-behavior	Yes	0.94	
area under the dynamic stress-temperature-curve	Yes	0.94	
hardness	Yes	0.91	good
failure energy acc. to **GRADY**	Yes	0.87	
dynamic **compression flow stress** at room temperature	Yes	0.86	
dynamic **tensile strength** at room temperature	Yes	0.84	
decline behavior from dynamic compression-stress-temperature-behavior	Yes	0.79	
decline behavior from dynamic stress-compression-behavior of compression-shear-test	Yes	0.61	insufficient
uniform elongation under dynamic loading	Yes	0.47	
CULVER-equation	Yes	0.02	impossible

FIG. 14. Sensitive properties of adiabatic shear failure.

When a qualitative consideration is fulfilled, a quantitative consideration is then reasonable and an assessment rating is definable. With this assessment rating, a ranking of propensities to the adiabatic shear failure behavior can be determined. A threshold value for the transition between the areas of shear failure and no shear failure can be defined because of the qualitative correlations. When this correlation is in agreement without an overlapping of data, the correlation is then usable for an assessment. For the failed materials, it is possible to define a quantitative correlation. Because of the level of the least square coefficient R^2 of the agreement, it is possible to create a ranking of material properties according to their significance to the adiabatic shear failure behavior, Fig. 14.

A very good correlation to the occurrence of adiabatic shear failure behavior shows the instability point (determined at stress-temperature-behavior), the shear strain from hat shaped test, and the area under the stress-temperature-curve. These are the properties governed by the effect of temperature and shear deformation. Pertaining to hardness, the failure energy according to Grady, the dynamic compression flow stress, the dynamic tensile strength and the decline-behavior of the stress-temperature-curve, are all feasible to directly correlate to the adiabatic shear behaviour. These properties are based on hardness, energy consumption, and strength. It is notable that material properties exist, which exhibit a greater correlation to the adiabatic shear failure behavior than the material's hardness. The decline- or softening behavior of the stress-strain-curve under compression-shear-loading and the uniform elongation under dynamic tensile loading, give an insufficient correlation. The failure criterion according to Culver shows only a qualitative, but no good quantitative correlation.

5. Conclusion

The aim of this study was to examine the influence of material properties on the local adiabatic shear failure behavior. The test results of the investigated quenched and tempered steels allowed an evaluation of the materials concerning their adiabatic shear failure propensity. The determination of the failure strain under adiabatic condition was performed with special inclined compression specimens in a so-called compression-shear test. These dynamic tests were carried out in a drop weight tower with initial strain rates of 200 1/s.

The most important material property for the analysis of the adiabatic failure behavior is the temperature-softening characteristic of the material. Therefore the strength level and the stress drop characteristics are crucial. Eventually the so-called instability point can be defined. This value gives a good agreement to the measured failure strain under biaxial adiabatic shear condition. Analytical studies with the use of the determined dynamic stress-temperature-behavior confirmed (by means of development of the stress resistance gradient)

the strong influence of the temperature softening behavior on the adiabatic shear failure.

The examined Culver-theory can only be used as a qualitative prediction for this material group. This theory is based on the linear softening behavior. The consideration of the shear fracture energy according to Grady gives both a qualitative as well as a good quantitative correlation to the measured shear failure behavior.

References

1. H. Tresca, *Sur la fluideite et lécoulement des corps solides*, Annales du conservatoire des arts et metiers, **41**, XI 1er fasc., 153–160, 1879.
2. C. Zener, J. H. Hollomon, *Effect of strain rate upon plastic flow of steel*, Journal of Applied Physics, **15**, 22–32, 1944.
3. H. C. Rogers, *Adiabatic shearing-general nature and material aspects, Material behavior under high stress and ultra-high loadings rates*, 29th Sagamore Army Materials Conf., J. Mescall and V. Weiss [Eds.], Plenum Press New York, Drexel University, Department of materials engineering, 101–118, 1983.
4. R. Dormeval, *The adiabatic shear phenomenon, Materials at high strain rates*, Elsevier Applied Science, T.Z. Blazynski [Ed.], 47–69, 1987.
5. Y. Xu, J. Zhag, Y. Bai, M. A. Meyers, *Shear localization in dynamic deformation: micro- structural evolution*, Metallurgical and Materials Transactions A, **39A**, 811–843, 2008.
6. R. Dormeval, *The adiabatic shear phenomena, Impact loading and dynamic behavior of materials*, Vol. 1, C. Y. Chiem, H. D. Kunze, L. W. Meyer [Eds.], DGM Informationsgesellschaft, Verlag, 43–56, 1988.
7. X. B. Wang, *Adiabatic shear localization for steels based on Johnson-Cook-Model and second- and fourth-order gradient plasticity models*, Journal of Iron and Steel Research, International, **14**, 56–61, 2007.
8. T. Pintat, B. Scholz, H. D. Kunze, O. Vöhringer, *The influence of carbon content and grain size on energy consumption during adiabatic shearing*, Journal de Physique, C3, **9**, 49, 237–244, 1988.
9. M. Edwards, *Properties of metals at high rates of strain*, Materials Science and Technology, **22**, 4, 453–462, 2006.
10. J. F. Mescall, *On the relative roles of strain-hardening and thermal softening in ASB*, Mechanical Engineering, Metallurgical application of shock-wave and high-strain-rate phenomena, **52**, 689–704, 1986.
11. J. Barry, G. Byrne, *Chip formation, acoustic emission and surface white layers in hard machining*, Annals of the CIRP, **51**, 65–70, 2002.
12. A. J. Bedford, A. L. Wingrove, K. R. L. Thompson, *The phenomenon of adiabatic shear deformation*, Journal of the Australian Institute of Metals, **19**, 1, 61–73, 1974.

13. Y. Meunier, R. Rouy, J. Moureaud, *Survey of adiabatic shear phenomena in armor steels with perforation*, Shock-wave and high strain rate phenomena in metals, 637–644, 1992.

14. A. G. Odeshi, S. Al-Ameeri, M. N. Bassim, *Effect of high strain rate on plastic deformation of a low alloy steel subjected to ballistic impact*, Journal of Materials Processing Technology, **162–163**, 385–391, 2005.

15. J. M. Yellup, R. L. Woodward, *Investigaion into the prevention of adiabatic shear failure in high strength armour materials*, Res. Mechanica, **1**, 41–57, 1980.

16. P. R. Guduru, A. J. Rosakis, G. Ravichandrian, *Dynamic shear bands: an investigation using high speed optical and infrared diagnostics*, Mechanics of Materials, **33**, 371–402, 2001.

17. A. Sabih, A. M. Elwazri, J. A. Nemes, S. Yue, *A workability criterion for the transformed ASB phenomena during cold heading of 1038 steel*, Journal of Failure and Prevention, **6**, 97–105, 2006.

18. N. Herzig, *Erfassung und Beschreibung des skalierten Fließ-, Verfestigungs- und Versagensverhalten ausgewählter metallischer Werkstoffe*, Dissertation, Schriftenreihe Band 004 Werkstoffverhalten, TU Chemnitz, Professur Werkstoffe des MB, 2008.

19. Z. G. Wang, G. Rittel, *Thermomechanical aspects of adiabatic shear failure of AM50 and Ti6Al4V alloys*, Mechanics of Materials, **40**, 8, 629–635, 2008.

20. Y. Bai, B. Dodd, *Adiabatic shear localization; Occurrence, theories and applications*, Pergamon press, Oxford, 1992.

21. E. Hanina, D. Rittel, Z. Rosenberg, *Pressure sensitivity of adiabatic shear banding in metals*, Applied physics letters, American institute of physics, **90**, 021915-1–021915-4, 2007.

22. R. S. Culver, *Thermal instability strain in dynamic plastic deformation*, Metallurgical effects at high strain rates, 519–529, 1973.

23. R. F. Recht, *Catastrophic thermoplastic shear*, Journal of Applied Materials, Transactions of the ASME, 189–193, 1964.

24. H. C. Rogers, *Adiabatic plastic deformation*, Ann. Rev. Mater. Sci., **9**, 283–311, 1979.

25. M. A. Meyers, *Dynamic behavior of materials*, Wiley-Interscience Publication; John Wiley and Sons, Inc., New York, 1994.

26. R. J. Clifton, *Material Response to ultra-high loadings rates*, Rep. NMAB - 356, NMAB, NAS, Washington, DC, Ch. 8, 1979.

27. T. W. Wright, *The physics and mathematics of ASB*, Cambridge University Press, 2002.

28. M. A. Meyers *et al.*, *Microstructural evolution in adiabatic shear localization in stainless steel*, Acta Materialia, **51**, 1307–1325, 2003.

29. M. R. Staker, *The relation between adiabatic shear instability strain and material properties*, Acta Metallurgica, **29**, 683–689, 1981.

30. J. R. Klepaczko, *Remarks on impact shearing*, Journal of Mechanics, Physics and Solids, **46**, 10, 2139–2153, 1998.

31. L. L. Wang, H. S. Bao, W. X. Lu, *The dependence of ASB in strain-rate, strain and temperature*, Journal de Physique, C3, **3**, 49, 207–214, 1988.

32. D. E. Grady, *Dissipation in adiabatic shear bands*, Mechanics of Materials, **17**, 289–293, 1994.

33. L. W. Meyer, L. Krüger, *Shear testing with hat specimen*, ASM Handbook, Mechanical Testing and Evaluation, ASM International, Materials Park, Ohio, **8**, 451–452, 2000.

34. J. F. Kalthoff, *Modes of dynamic shear failure in solids*, International Journal of Fracture, **101**, 1–31, 2000.

35. L. W. Meyer, L. Krüger, S. Abdel–Malek, *Adiabatische Schervorgänge*, Materialprüfung, **41**, 31–35, 1999.

36. L. W. Meyer, E. Staskewitsch, A. Burblies, *Adiabatic shear failure under biaxial dynamic compression/shear loading*, Mechanics of Materials, **17**, 203–214, 1994.

37. L. W. Meyer, L. Krüger, *Drop-weight compression shear testing*, ASM Handbook, Mechanical Testing and Evaluation, ASM International, Materials Park, Ohio, **8**, 452–454, 2000.

38. X. Sun, W. Liu, W. Chen, D. Templeton, *Modeling and characterization of dynamic failure of borosilicate glass under compression/shear loading*, Int. Journal of Impact Engineering, **36**, 226–234, 2009.

39. L. W. Meyer, E. Staskewitsch, *Adiabatic shear failure of the titanium alloy Ti6Al4V under biaxial dynamic compression/shear loading*, Shock Waves and high-strain-rate phenomena in metals, 1939–1946, 1992.

40. K. H. Hartmann, H. D. Kunze, L. W. Meyer, *Metallurgical effects on impact loaded materials*, Shock waves and high strain rate phenomena in metals, concepts and applications, Plenum Press New York, 325–337, 1981.

41. J. R. Klepaczko, B. Rezaig, *A numerical study of ASB in mild steel by dislocation mechanics based constitutive relations*, Mechanics of Materials, **24**, 125–139, 1996.

42. H. Feng, M. N. Bassim, *Finite element modeling of the formation of ASB in AISI 4340 steel*, Material Science and Engineering, **A266**, 255–260, 1999.

43. L. W. Meyer, S. Manwaring, *Critical adiabatic shear strength of low alloyed steel under compressive load*, Metallurgical applications of shock-wave and high-strain-rate phenomena, 657–674, 1986.

44. L. W. Meyer, *Adiabatic shear failure at biaxial dynamic compression/shear loading*, Euromech, **282**, 1991.

45. S. N. Medyanik, W. K. Liu, S. Li, *On criteria for dynamic adiabatic shear band propagation*, Journal of the Mechanics and Physics of Solids, **55**, 1439–1461, 2007.

46. L. E. Murr, *Applications of extreme deformation*, Materials Technology, **22**, 4, 193–199, 2007.

Received December 18, 2010; revised version May 31, 2011.

ENGINEERING TRANSACTIONS • *Engng. Trans.* • **59**, 2, 85–100, 2011
Polish Academy of Sciences • Institute of Fundamental Technological Research (IPPT PAN)
National Engineering School of Metz (ENIM)

THE STATIC AND DYNAMIC COMPRESSIVE BEHAVIOUR OF SELECTED ALUMINIUM ALLOYS

R. W i n z e r, A. G l i n i c k a

Warsaw University of Technology
Faculty of Civil Engineering
Department for Strength of Materials
16 Armii Ludowej Av., 00-637 Warsaw, Poland
e-mail: {r.winzer, a.glinicka}@il.pw.edu.pl

The mechanical properties of structural aluminium alloys EN AW-5083 and EN AW-6082 in the 'H111' and 'T6' conditions, respectively, subjected to compressive loadings in the quasi-static and dynamic strain rate regimes, are investigated. Both alloys are used as structural components not only in car body design or ship building, but also in civil engineering. Therefore, compression tests at room temperature were conducted using a servohydraulic Instron machine, in order to determine the materials' behaviour at low and intermediate rates of deformation. In addition, to predict the dynamic response of these materials, the Split Hopkinson Pressure Bar (SHPB) technique was utilized. For alloy 5083-H111, a changeover from negative to positive strain rate sensitivity at dynamic strain rates is observable, whilst alloy 6082-T6 exhibits a mild trend towards positive strain-rate sensitivity. Furthermore, the coefficients of the Johnson-Cook model, that are valid under dynamic conditions, are determined. The finite element simulation of SHPB experiments shows that the constitutive model represents the materials' behaviour quite well.

1. Introduction

Aluminium alloys are a flexible and attractive material for use in many applications. The desire for optimal design of structures with high mechanical capacity and light-weight properties, does not only play a significant role in aerospace engineering. In view of shorter becoming supply of resources, the aspect of minimisation of weight is also crucial in car manufacturing and ship-building. Therefore, light-weight materials like aluminium alloys are already applied as structural materials during the design process. Moreover, automotive crashworthiness plays an important role in the design of passenger cars. In order to manage the energy of a collision in a reliable manner in the event of a car accident or ship collision, the energy absorption performance needs to be understood. Thus, the stress-strain relationship for dynamic strain rates should be studied.

Due to its high ratio of load-bearing capacity to weight combined with high corrosion resistance, what leads to lower maintenance requirements, aluminium alloys are also used in civil engineering. In addition, thanks to its recycling potential, it is a sustainable solution as a building material. Indeed, a classical field of aluminiums‘ utilisation in civil engineering is its application as facade elements [1], but load-bearing aluminium structures can also be found [2], for example in bridge constructions. It can be determined that aluminium structures in civil engineering are subjected to loadings caused by wind, earthquake and impact, for instance. These loadings generate strain rates from 10^{-4} up to 10^{4} s^{-1}. Therefore, the material properties of two commercial aluminium alloys EN AW-5083 and EN AW-6082 in the ‘H111’ and ‘T6’ condition, respectively, at low and high rates of deformation are investigated. As mentioned in [3], the series 5*xxx* and 6*xxx* are most used for structural components in bridge building. Eurocode 9 [4] states that the first alloy is the strongest structural non-heat treatable alloy in general commercial use, possessing very good corrosion resistance in the marine environment. Therefore, it is utilised for structural parts of naval and offshore structures. On the other hand, the second alloy is one of the most widely used heat treatable high strength alloy with good corrosion resistance and good weldability.

Alloy composition, strain rate and temperature may have an effect on mechanical properties of aluminium alloys [5]. Wagenhofer *et al.* [6] reported a reversed strain effect occurring at room temperature in alloy 5086. A negative strain rate sensitivity changed into a positive one at a strain rate nearly equal to 1 s^{-1}. Similarly, Clausen *et al.* [7] revealed that alloy 5083 in ‘H116’ condition exhibits a negative strain rate sensitivity for strain rates up to 1 s^{-1}, but positive strain rate sensitivity in the dynamic strain rate regime. A changeover from negative to mild positive strain rate was also observed by Hadianfard *et al.* [8] for 5*xxx* aluminium alloys. Aforementioned investigations considered the alloys’ behaviour in tension. On the contrary, Chen *et al.* [9] carried out experimental tests over a wide range of strain rates on 6*xxx* aluminium alloys in tension, namely on alloys 6060 and 6082 in tempers T6. The tests showed that both alloys exhibit only slight strain rate sensitivity, even a slight negative tendency for high strain rates is observable for both alloys, whilst Lee and Kim [10] disclosed that the flow stress of alloy 6061 in temper T6 exhibits an increase of 320 and 90% at compression and tension, respectively, for high rates of deformation. A distinctive sensitivity to the strain rate is visible. Thus, the objective of underlying work is to investigate the effects of strain rate on the mechanical properties of selected 5*xxx* and 6*xxx* aluminium alloys in compression. Hence, compression tests at room temperature were conducted using a servo-hydraulic Instron machine in order to determine the materials‘ behaviour at low and intermediate rates of deformation. In addition, to predict the response

caused by impact loading, the Split Hopkinson Pressure Bar (SHPB) technique was utilised. Moreover, for further FE analysis in future, constitutive material parameters were determined and validated.

2. Experimental procedure

2.1. The investigated materials

As mentioned above, the aluminium alloys EN AW-5083 and EN AW-6082 in tempers H111 and T6, respectively, were considered in this evaluation. Their main alloying elements are magnesium, manganese and silicium, magnesium. The chemical compositions of the materials are presented in Table 1. The alloys were provided as round bars with 16 or 10 mm diameters.

Table 1. Chemical compositions of the alloys in wt.%.

Alloy	Si	Fe	Cu	Mn	Mg	Cr	Zn	Ti
EN AW-5083	0.40	0.40	0.10	0.70	4.45	0.25	0.25	0.15
EN AW-6082	0.88	0.29	0.08	0.46	0.73	0.03	0.04	0.02

2.2. Static and quasi-static compression tests

Compression tests were carried out using a servohydraulic Instron machine (type 8802) at strain rates of 10^{-4}, 10^{-3}, 10^{-2}, 10^{-1} and 1 s^{-1}, at room temperature. All tests were performed in displacement control with clamp velocity adapted to the corresponding strain rate. In order to specify a flow curve for cylindrical shaped metallic specimens, the initial ratio between length and diameter should be between 1 and 2. The samples' ratio was equal to 1.5 with an initial diameter of 10 mm in all cases. Three compression tests were at least conducted for each strain rate and alloy.

2.3. Dynamic compression tests

A variety of experimental techniques, such as Taylor impact or shock loading by plate impact, can be utilised to obtain high rates of strain. An interesting and detailed overview of these techniques can be found in [11]. A technique which enables to measure the response of materials at strain rates between 10^2–10^4 s^{-1}, first introduced by Kolsky [12], is the Split Hopkinson Pressure Bar (SHPB) apparatus. In general, this apparatus consists of an air gun, a striker bar, two Hopkinson bars (known as incident and transmitter bars), a velocity measuring device and recording equipment. The specimen is sandwiched between the two

bars. The dynamic compression tests were performed in the laboratory of the Division of Experimental Mechanics at the Institute of Fundamental Technological Research.

A schematic view of the SHPB apparatus is illustrated in Fig. 1. Both the incident and transmitter bars are made of spring steel, whose yield strength and elastic modulus are equal to 1180 MPa and 210 GPa, respectively. Their diameter and length are 20 and 1050 mm, respectively. The striker bar or projectile has the identical diameter and is made of the same steel. Three striker bars of varying length were used.

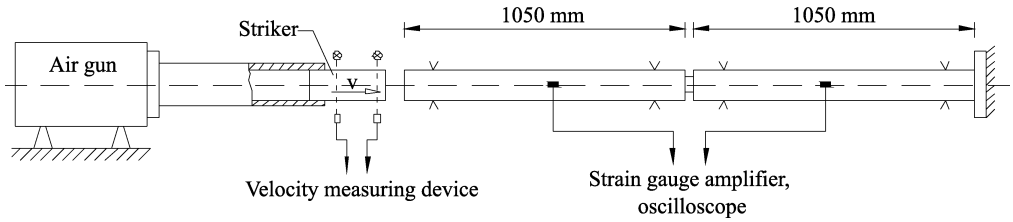

FIG. 1. Schematic view of SHPB apparatus.

First of all, the striker bar is fired by the air gun and impacts the incident bar. By reason of the impact, a nearly rectangular compressive stress and a strain pulse with very short rise time is generated, which propagates with the speed of sound $c_0 = (E/\rho)^{1/2}$ along the incident bar until it hits the specimen, where E is the elastic modulus and ρ the bar's density. Propagating into the specimen, a part is transmitted into the transmitter bar, whilst the other part is reflected back into the incident bar as a tensile wave. During the test, the bars remain within their elastic limit. The incident, transmitted and reflected pulses ε_I, ε_T, and ε_R, respectively, were measured using strain gauges (HBM LY11-1.5/120) attached to each bar. The strain gauges were connected with a strain gauge amplifier. Finally, the output signals of the strain gauges were visualized and stored in an oscilloscope (Agilent 54624A) at a sampling rate of 0.25 μs. Figure 2 shows typical incident, transmitted and reflected voltage signals that were saved into the oscilloscope. The time-dependent strain rate can be determined by means of recorded strains as follows:

$$\dot{\varepsilon}_s = -\frac{2c_0}{l_0}\varepsilon_R, \tag{2.1}$$

where l_0 is the initial length of the specimen. Thus, the strain as a function of time can be calculated by integrating the above equation from 0 to t,

$$\varepsilon_s = -\frac{2c_0}{l_0}\int_0^t \varepsilon_R d\widetilde{t}. \tag{2.2}$$

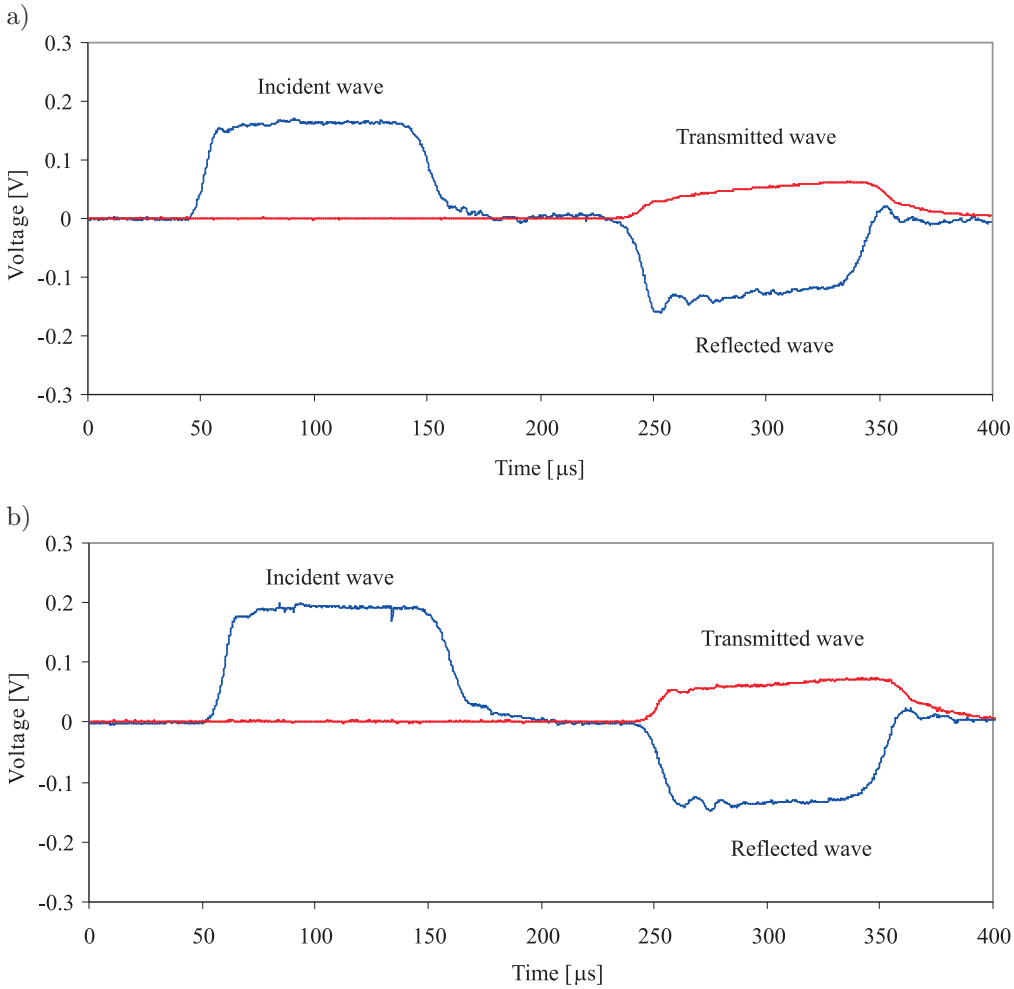

FIG. 2. Typical pulses for (a) 5083-H111 and (b) 6082-T6 aluminium alloy.

Considering force equilibrium at the contact faces of the bars, an average value for the stress on the specimen can be derived

$$\sigma_s = E\frac{A_b}{A_s}\varepsilon_T, \tag{2.3}$$

where A_b is the cross-sectional area of the incident bar and A_s is the cross-sectional area of the specimen.

A detailed derivation of Eqs. (2.1)–(2.3) can be found elsewhere [13, 14]. From the theoretical point of view, they are based on the one-dimensional propagation of elastic waves in a continuum including some basic assumptions. Namely, there exists force equilibrium on the interfaces during the process of deformation, i.e.

a uniform axial stress distribution is assumed, and both the friction and inertia forces are negligible. In order to reduce frictional effects, the interfaces between the specimen and the bars were lubricated. As recommended in [14, 15], to minimise the errors due to longitudinal and radial inertia forces, all specimens had an initial diameter and length of 10 and 5 mm, respectively. A special instrumentation was used to apply the specimen in the center of the bars. A further assumption is that the elastic wave travels along the bars without any damping. This is justified only if the ratio between wavelength and bar diameter is great enough, otherwise dispersion is clearly visible as shown by GORHAM and WU [16].

3. Results of static and dynamic compression tests

Henceforth, the nominal (engineering) strain and stress are used to calculate the true strain $\varepsilon = \ln(1+\varepsilon_{\text{nom}})$ and the true stress $\sigma = \sigma_{\text{nom}}(1+\varepsilon_{\text{nom}})$. Figure 3 illustrates representative flow curves obtained during low and intermediate strain rate compression tests at room temperature. A considerable different trend is observed. For alloy 5083-H111, a negative strain rate effect is clearly visible, i.e. with increasing strain rate, a decreasing flow stress level is observable. For instance, at a plastic strain of 0.3 the flow stress decreased approximately by 15%. In contrast, a slight trend towards positive strain rate sensitivity for alloy 6082-T6 is shown, but this effect is not so distinctive as in the case of the previous alloy. Only an increase of nearly 3.5% could be found.

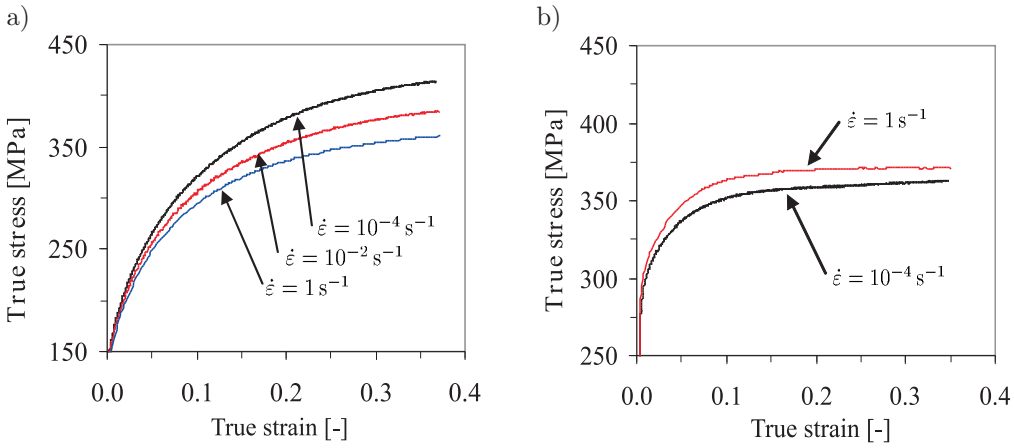

FIG. 3. Static flow curves of (a) 5083-H111 and (b) 6082-T6 aluminium alloy.

Furthermore, several tests have been conducted for each alloy by means of the SHPB apparatus. In Fig. 4, the obtained dynamic flow curves are illustrated.

For the sake of clarity, only hardening curves corresponding to low, intermediate and high impact velocities are shown. The maximum strain did not exceed the value of 0.4, whereas strain rates from 500 up to 5500 s^{-1} have been achieved. Figure 4a clearly reveals that the flow stress level of aluminium alloy 5083-H111 increases with increasing strain rate. A change in the strain rate sensitivity can be recognized. The flow stress level of alloy 6082-T6 also increases with increasing strain rate, but very slightly. For a more precise analysis, the flow stress level at 0.05 true plastic strain is plotted as a function of strain rate in Fig. 5. A reduction of flow stress for alloy 5083-H111 can be clearly observed

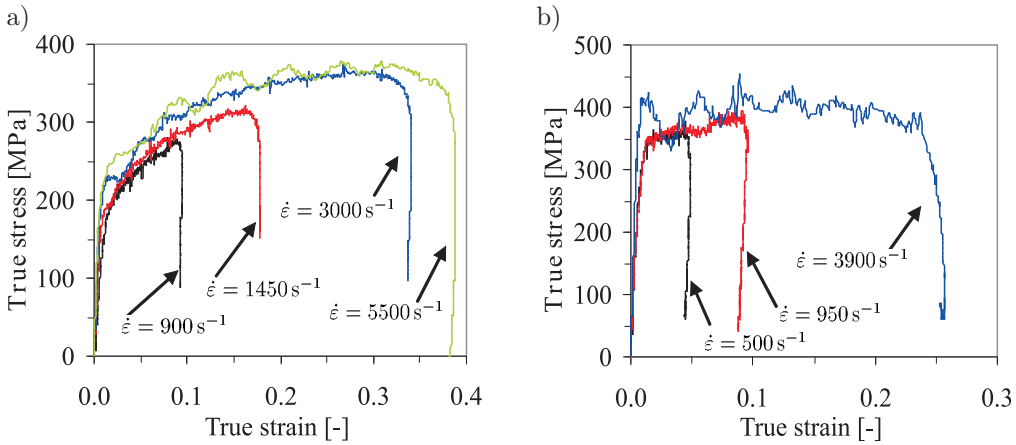

FIG. 4. Dynamic flow curves of (a) 5083-H111 and (b) 6082-T6 aluminium alloy.

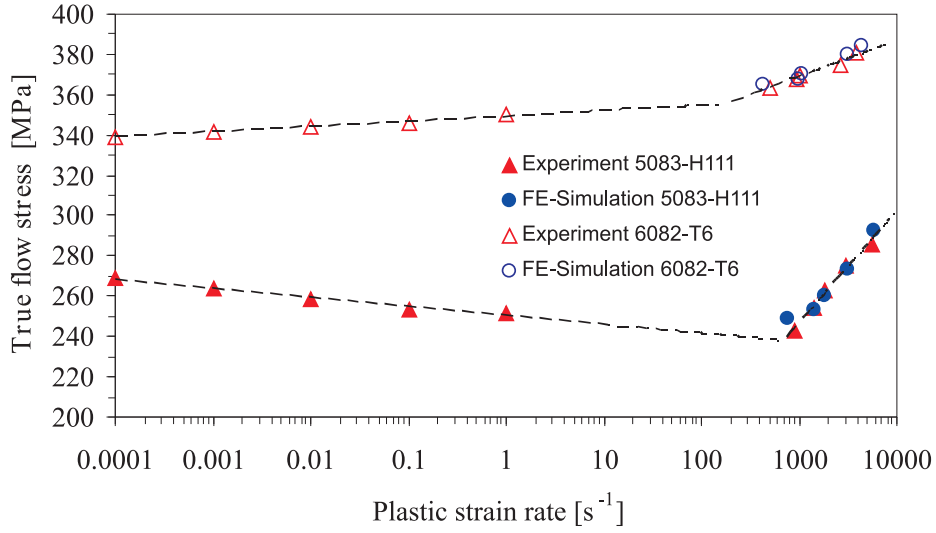

FIG. 5. True flow stress at 0.05 true plastic strain as a function of strain rate; comparison of numerical results.

for strain rates between 10^{-4} and 1 s^{-1}. A decrease of approximately 10% could be found out. However, under dynamic conditions, the flow stress increases by about 25%. In contrast, aluminium alloy 6082-T6 is almost rate-insensitive, a decrease of nearly 3% at quasi-static strain rates is observed. A mild trend towards positive strain rate sensitivity can be noticed. The flow stress increased by about 8% under dynamic conditions.

Furthermore, the diameter of each specimen was measured prior and after the experiment in two or three radial directions. It was found out that the surface had a circular shape, i.e. not elliptical. This indicates that the alloys behave as isotropic. Therefore, the use of an isotropic yield criterion for numerical purposes is justified. Typical specimens are shown in Fig. 6. For samples B and C, strain rates of 950 and 3000 s^{-1} were calculated, their corresponding dynamic hardening curves are plotted in Fig. 4. Their initial and final lengths were 4.94, 4.98 and 3.48, 4.58 mm, respectively, what leads to a maximum strains of 0.35 and 0.08, respectively.

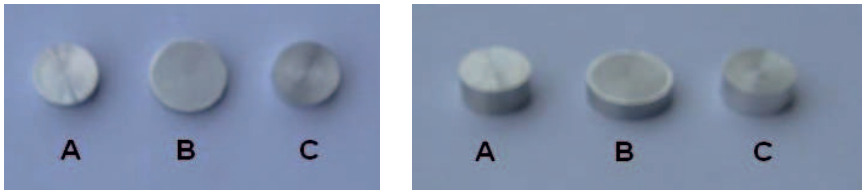

FIG. 6. Examples of typical specimens used for dynamic investigations, prior to experiment (A), and aluminium alloy 5083-H111 (B) and 6082-T6 (C) samples after compression.

4. NUMERICAL SIMULATIONS

In order to verify the constitutive model, a finite element simulation of the Hopkinson bar test was performed. Since stress wave propagation is a typical application for an explicit finite element code, the commercial software ABAQUS/Explicit, well-suited for high-speed dynamic events [17], was used.

4.1. Basic formulations, constitutive equation and parameter identification

When the elastic strains are small (negligible compared to unity) in a large deformation analysis, the additive decomposition of the rate-of-deformation tensor into elastic and plastic parts is assumed (see, e.g. BELYTSCHKO *et al.* [18])

$$\mathbf{D} = \mathbf{D}^e + \mathbf{D}^p, \tag{4.1}$$

where $\mathbf{D}$ is defined as the symmetric part of the velocity gradient as follows:

$$\mathbf{D} = \operatorname{sym} \mathbf{L} = \operatorname{sym} \frac{\partial v}{\partial x}. \tag{4.2}$$

Henceforth, a hypoelastic-viscoplastic isotropic material is considered. Then, ABAQUS computes the plastic part of the rate-of-deformation tensor by means of the associated flow rule:

$$\mathbf{D}^p = \lambda \frac{\partial f}{\partial \boldsymbol{\sigma}} = \frac{3}{2} \frac{\overline{\varepsilon}^p}{\overline{\sigma}} \mathbf{s}. \tag{4.3}$$

In this equation $\mathbf{s}$ is the deviatoric part of the stress tensor, whilst $\overline{\varepsilon}^p$ is the equivalent plastic strain. To characterise the yield behaviour of metals, what means incompressible behaviour beyond the elastic limit, a yield function of von Mises type is considered

$$f = \sqrt{\frac{3}{2}} ||\mathbf{s}|| - \overline{\sigma}. \tag{4.4}$$

To ensure objectivity, the finite element programme uses a linear hypoelastic relation based on the Green-Naghdi stress rate tensor

$$\boldsymbol{\sigma}^{\nabla G} = \dot{\boldsymbol{\sigma}} - \boldsymbol{\Omega} \cdot \boldsymbol{\sigma} + \boldsymbol{\sigma} \cdot \boldsymbol{\Omega} = \mathbb{C} : \mathbf{D}^e, \tag{4.5}$$

where $\boldsymbol{\Omega}$ and $\mathbb{C}$ are the angular velocity tensor and the fourth-order elastic stiffness tensor, respectively. Moreover, the plastic behaviour of the specimen as a function of strain, strain rate and temperature can be specified by the Johnson-Cook constitutive equation [19]. In particular, this constitutive relation reads

$$\overline{\sigma} = (A + B(\overline{\varepsilon}^p)^n) \left(1 + C \ln \left(\frac{\dot{\overline{\varepsilon}}^p}{\dot{\varepsilon}_0}\right)\right) (1 - \widehat{T}^m). \tag{4.6}$$

The term in the last parenthesis accounts for thermal softening of the material. In the case of T_r and T_m being the room and melting temperature, respectively, then $\widehat{T}$ is defined as

$$\widehat{T} = \frac{T - T_r}{T_m - T_r}. \tag{4.7}$$

As mentioned in [9], investigations by Clausen *et al.* [7] and Børvik *et al.* [20] revealed that a temperature rise up to 100°C does not affect the mechanical behaviour in a critical manner. An estimation of the temperature rise in this work is found to be 38°C. Due to the latter and the fact that all tests were carried out at room temperature, $\widehat{T}$ was set a priori equal to zero. In order to determine the other coefficients, a reference stress-strain curve with a reference strain rate needs to be chosen. Thus, the parameter $\dot{\varepsilon}_0$ is determined. The reference strain rate for alloys 5083-H111 and 6082-T6 were chosen to be 1450 and 1000 s^{-1}, respectively. Afterwards, the coefficients in the first parenthesis can be determined, whereas the value of A can be identified as the yield stress.

In the next step, B and n can be calculated by means of the least square method. Aforementioned procedure was repeated for each test, so all stress-strain curves have analytical forms. Finally, the parameter C can be specified by rearranging Eq. (4.6) with respect to parameter C. The parameters for the alloys are listed in Table 2, but one should note the following: namely, since C must have a positive value due to the fact that selected model requires a positive strain rate the use of the model is only justified for situations where dynamic strain rates emerge. So, negative strain rate sensitivity of alloy 5083-H111 in the static and quasi-static dynamic strain rate regime cannot be modelled via the determined coefficients. Moreover, it is possible to ascertain additional Johnson-Cook parameters for alloy 6082-T6 that are valid for low and intermediate rates of deformation, but within this strain rate regime the alloy can also be modelled as rate-insensitive. The experimental results show that this alloy exhibits only a slight sensitivity to the strain rate (cf. Fig. 4b); therefore, the coefficient has only a slight value.

Table 2. Parameters in the Johnson-Cook constitutive equation.

Alloy	A [MPa]	B [MPa]	n [–]	C [–]
EN AW- 5083	147.0	349.2	0.396	0.104
EN AW- 6082	307.8	145.7	0.288	0.02519

4.2. Finite element model and numerical results

In general, the model consists of two elastic bars with a Young's modulus of 210 GPa and Poisson's ratio equal to 0.3, and a specimen which is sandwiched between these two bars. A third bar (striker bar) hits the free end of the incident bar. This experimental setup was modelled taking the double symmetry into account (cf. Fig. 7). Eight-node hexahedron elements with reduced integration were used to model all parts. A surface to surface contact was considered between the respective interfaces.

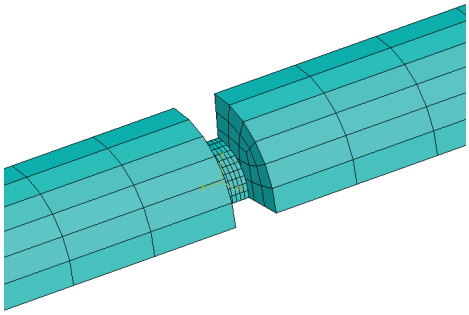

FIG. 7. Finite element mesh of SHPB setup.

The initial compressive stress wave can be simulated via the impact of the striker bar at the free end of the incident bar. Another possibility is to subject the free end of the bar to a blast load. Both possibilities have been performed leading to the same results. Moreover, the analytical solution of one-dimensional wave equation assumes that the specimen is subjected to a Heaviside step load of an infinite duration. Indeed, this zero rise time assumption is not realistic. In practice, however, the pulse shape is trapezoidal and is distorted as a result of wave dispersion. As shown in Fig. 8b, in the time domain, dispersion is observable as oscillations. Thus, using finite element simulation, the pulse shape caused by the impact or rather the blast load should be trapezoidal. RAMÍREZ and RUBIO–GONZALEZ [21] demonstrated that the higher, is the rise time, the lower will be the dispersion effects. This is important, since wave dispersion is able to limit the accuracy of the obtained results, especially for lower impact velocities, where the rise time during the experiment takes a longer period. The pulse shape effect on wave dispersion is presented in Fig. 8, a longer rise time leads to reduced dispersion effects. A trapezoidal blast load fits better to experimental data and is, therefore, more realistic (cf. Fig. 8b). Earlier observations in [21] are in good agreement with experimental and numerical results of this work.

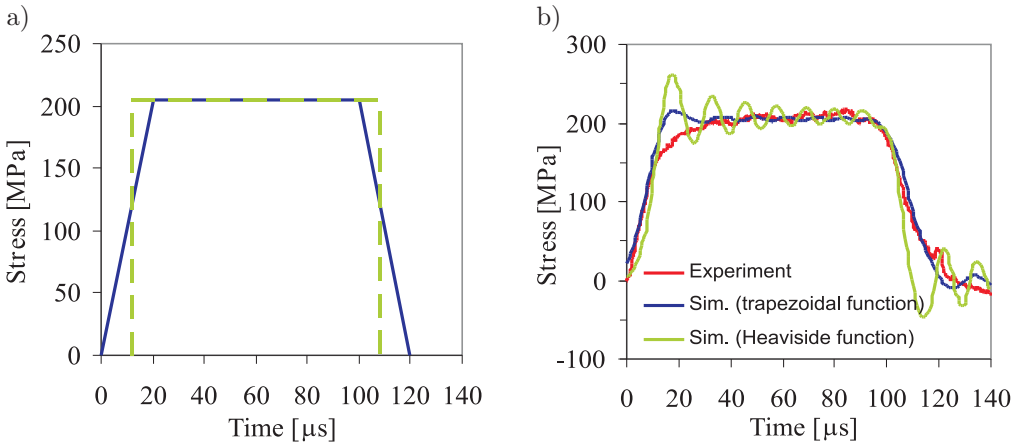

FIG. 8. (a) Trapezoidal and Heaviside step load, (b) comparison between experimental and simulated incident pulses.

All tests for each alloy have been simulated. In general, the numerical results represent the experimental findings with adequate accuracy. In Fig. 9 a comparison between numerical and experimental results for both alloys is presented, their stress-strain relations were already presented in Fig. 4. All strain pulses are simulated reasonably well, as shown in Fig. 9a-c. The aforementioned pulses are

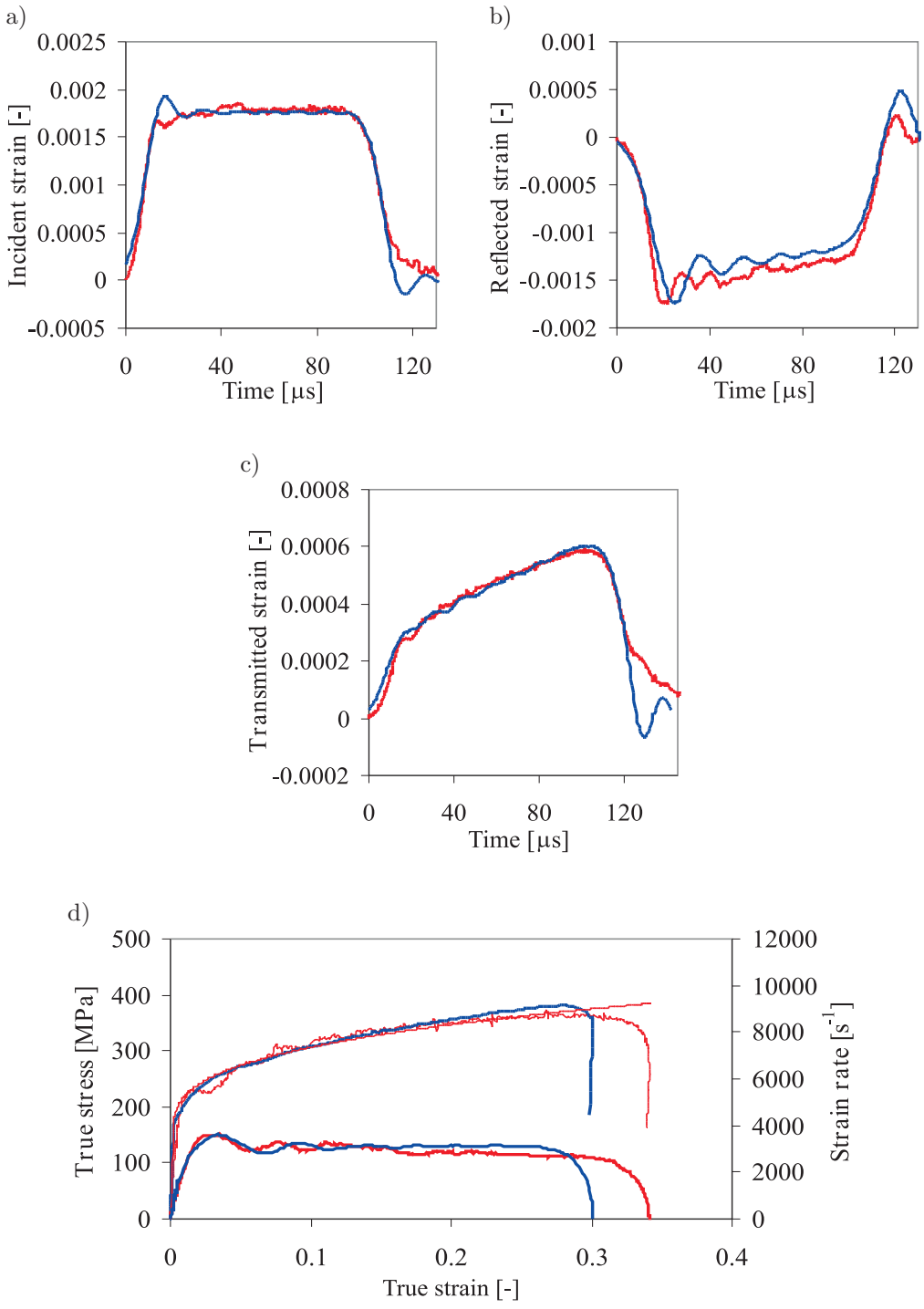
a)
Incident strain [-]
0.0025
0.002
0.0015
0.001
0.0005
0
-0.0005
0
40
80
120
Time [μs]
b)
Reflected strain [-]
0.001
0.0005
0
-0.0005
-0.001
-0.0015
-0.002
0
40
80
120
Time [μs]
c)
Transmitted strain [-]
0.0008
0.0006
0.0004
0.0002
0
-0.0002
0
40
80
120
Time [μs]
d)
True stress [MPa]
500
400
300
200
100
0
12000
10000
8000
6000
4000
2000
0
Strain rate [s-1]
0
0.1
0.2
0.3
0.4
True strain [-]

[FIG. 9a-d]

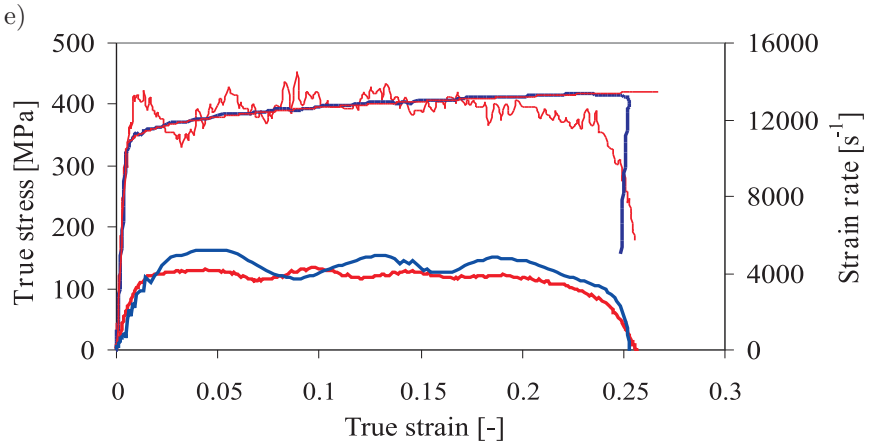

FIG. 9. Comparison between (red line) experimental and (blue line) numerical results; representative (a) incident, (b) reflected, (c) transmitted strain pulse, (d) stress-strain and strain rate-strain curve for alloy 5083-H111 and (e) stress-strain and strain rate-strain curve for alloy 6082-T6.

related to Fig. 9d, whilst in Fig. 9e only the dynamic hardening curve with the corresponding strain rate-strain relation for alloy 6082-T6 is presented. In case of alloy 5083-H111, the obtained maximum strains in the finite element simulations are slightly shorter compared to the experimental strains, whilst in case of the other alloy, both strains agree much better. Nevertheless, it can be observed that the Johnson-Cook model represents the flow stress level of both alloys quite well. All this can be confirmed when Fig. 5 is considered. The flow stress obtained by the experiments and simulations at 0.05 true plastic strain, can be compared with each other at a wide range of strain rates. A good agreement with the experimental data is observable.

5. Conclusions

Compression tests on two structural aluminium alloys over a wide range of strains and strain rates were performed. To obtain quasi-static strain rates, a servohydraulic Instron machine was utilised, whilst a Split Hopkinson Pressure Bar was applied in order to obtain high strain rates.

The experimental findings reveal that the alloy 5083 in temper H111 exhibits a negative strain rate sensitivity in the quasi-static strain rate regime, whilst a positive strain rate sensitivity is observable in the dynamic strain rate regime. Alloy 6082 in temper T6 is almost rate-insensitive for strain rates up to 1 s^{-1}. Above this strain rate, a slight positive strain rate sensitivity can be noticed. Unfortunately, an exact value of the turning point in case of alloy 5083-H111

could not be determined due to lack of experimental data in the range of 10–500 s^{-1}. A logarithmic interpolation through the data points in Fig. 5 would lead to a value of approximately 600 s^{-1}. To achieve this intermediate or "sub-Hopkinson" strain rates, a servohydraulic machine must be used which enables higher clamp velocities. However, as mentioned by other authors [6, 8], the two test devices, namely the servohydraulic machine in conjunction with the SHPB apparatus, can be applied in order to obtain consistent experimental data. Despite the lack of experimental data it is visible to the naked eye (cf. Fig. 5) that intermediate strain rate data points fit well with data points in the dynamic strain rate regime. No sudden change in the flow stress level indicating a source of error is visible.

Moreover, the parameters in the Johnson-Cook constitutive equation were calibrated (cf. Table 2). Since it is not possible to simulate negative strain rate sensitivity by means of this model, the calculated parameters are only valid under dynamic conditions, i.e. for strain rates above ca. 500 s^{-1}. In case of alloy 6082-T6, the parameters are also valid under dynamic conditions, this means for strain rates exceeding the value of ca. 100 s^{-1}. For strain rates below 100 s^{-1} this alloy can be modelled as rate-insensitive. In order to validate the constitutive model, a finite element simulation of the Split Hopkinson Pressure Bar test was performed. Both the strain hardening and strain rate hardening could be represented via this model adequately. It can be determined that the numerical results fit very well to the experimental data.

Acknowledgements

Support for the present work was provided by the Warsaw University of Technology under rector's grant no. 503G 1083 0100 009. Furthermore, the authors would like to thank Dr. Artur Zbiciak for numerous and fruitful discussions and Professor Zbigniew L. Kowalewski for giving them the opportunity to conduct their dynamic experiments in the laboratory of the Division of Experimental Mechanics, at the Institute of Fundamental Technological Research.

References

1. H. Wilquin, *Aluminium in Building – Construction and Design* [in German], Birkhäuser Verlag für Architekten, Berlin, 2001.
2. G. Valtinat, *Aluminium in Structural Engineering* [in German], Ernst & Sohn, 2003.
3. T. Siwowski, *Aluminium road bridges – past, present and future* [in Polish], *Drogi i Mosty*, **1**, 39–73, 2005.

4. Eurocode 9, ENV 1999-1-1, *Design of aluminium structures – Part 1.1: General rules – General rules and rules for buildings*, 1997.

5. A. M. Bragov and A. K. Lumanov, *Elastoplastic Properties of Aluminum Alloy AMg6 with High Strain Rates*, Journal of Applied Mechanics and Technical Physics, **5**, 755–758, 1988.

6. M. Wagenhofer, M. Erickson–Natishan, and R. W. Armstrong, *Influences of strain rate and grain size on yield and serrated flow in commercial Al-Mg alloy 5086*, Scripta Materialia, **41**, 1177–1184, 1999.

7. A. H. Clausen, T. Børvik, O. S. Hopperstad, and A. Benallal, *Flow and fracture characteristics of aluminium alloy AA5083-H116 as function of strain rate, temperature and triaxiality*, Materials Science and Engineering A, **364**, 260–272, 2003.

8. M. J. Hadianfard, R. Smerd, S. Winkler, and M. Worswick, *Effects of strain rate on mechanical properties and failure mechanism of structural Al-Mg alloys*, Materials Science and Engineering A, **492**, 283–292, 2008.

9. Y. Chen, A. H. Clausen, O. S. Hopperstad, and M. Langseth, *Stress-strain behaviour of aluminium alloys at a wide range of strain rates*, International Journal of Solids and Structures, **46**, 3825–3835, 2009.

10. O. S. Lee and M. S. Kim, *Dynamic material property characterization by using Split Hopkinson pressure bar (SHPB) technique*, Nuclear Engineering and Design, **226**, 119–125, 2003.

11. J. E. Field, W. G. Walley, W. G. Proud, H. T. Goldrein, and C. R. Siviour, *Review of experimental techniques for high rate of deformation and shock studies*, International Journal of Impact Engineering, **30**, 725–775, 2004.

12. H. Kolsky, *An Investigation of the Mechanical Properties of Materials at Very High Rates of Loading*, Proceedings of the Physical Society of London, **B62**, 676, 1949.

13. M. A. Meyers, *Dynamic Behavior of Materials*, New York, John Wiley & Sons, Inc., 1994.

14. M. M. Al–Mousawi, S. R. Reid, and W. F. Deans, *The use of the split Hopkinson pressure bar techniques in high strain rate materials testing*, Proceedings of the Institution of Mechanical Engineers, Part C: Journal of Mechanical Engineering Science, **211**, 273–292, 1996.

15. E. D. H. Davies and S. C. Hunter, *The dynamic compression testing of solids by the method of split Hopkinson pressure bar*, Journal of the Mechanics and Physics of Solids, **11**, 155–181, 1963.

16. D. A. Gorham and X. J. Wu, *An empirical method for correcting dispersion in pressure bar measurements of impact stress*, Measurements Science and Technology, **7**, 1227–1232, 1996.

17. ABAQUS/Explicit Manual, *Getting Started with ABAQUS*, Version 6.9.

18. T. Belytschko, W. K. Liu, and B. Moran, *Nonlinear Finite Elements for Continua and Structures*, Chichester, John Wiley & Sons, Inc., 2000.

19. G. R. Johnson and W. M. Cook, *A Constitutive Model and Data for Metals Subjected to Large Strains and High Temperatures*, [in:] Proceedings of the Seventh International Symposium on Ballistic, Hague, The Netherlands, 1983.

20. T. Børvik, A. H. Clausen, M. Eriksson, T. Berstad, O. S. Hopperstad, and M. Langseth, *Experimental and numerical study on the perforation of AA6005-T6 panels*, International Journal of Impact Engineering, **32**, 35–64, 2005.

21. H. Ramírez and C. Rubio–Gonzalez, *Finite-Element simulation of wave propagation and dispersion in Hopkinson bar test*, Materials & Design, **27**, 36–44, 2006.

Received December 23, 2010; revised version June 9, 2011.

ENGINEERING TRANSACTIONS • *Engng. Trans.* • **59**, 2, 101–117, 2011
Polish Academy of Sciences • Institute of Fundamental Technological Research (IPPT PAN)
National Engineering School of Metz (ENIM)

MECHANICAL CHARACTERIZATION OF STEEL FOR FASTENING IN A WIDE RANGE OF STRAIN RATE

E. Cadoni[1)], A.M. Bragov[2)], M. Dotta[1)], D. Forni[1)], A. Konstantinov[2)], A. Lomunov[2)], A. Ripamonti[3)]

[1)] **University of Applied Sciences of Southern Switzerland**
DynaMat Laboratory
Switzerland

[2)] **State University of Nizhny Novgorod**
Research Institute of Mechanics
Russia

[3)] **Agrati Group S.p.A.**
Italy

In this paper, the preliminary results of the mechanical characterization in a wide range of strain rate of the 30MnB4 steel, usually adopted for fasteners, are described. In this study the different issues required to implement the dynamic test results in numerical code have been analyzed. Different experimental techniques have been used for different strain rates: universal machine, Hydro-Pneumatic Machine, JRC-Modified Hopkinson Bar and Split Hopkinson Pressure Bar. The failure at high strain rate has been examined by means of fast digital image recording systems. The material shows enhanced mechanical properties increasing the strain rate: this fact can be taken into consideration to improve the product design and the manufacturing process. The experimental research has been developed in the DynaMat laboratory of the University of Applied Sciences of Southern Switzerland and in the Laboratory of Dynamic Investigation of Materials in Nizhny Novgorod, in the frame of the Swiss – Russian Joint Research Program.

1. Introduction

The fastening technology is of capital importance in the transport fields (aeronautic, automotive, etc.). Thanks to the development of advanced modeling tools, as FE codes, it is now possible to study the manufacturing process of fasteners, which are, for some aspects, similar to impacts (forming loads are applied in fraction of seconds). Such advanced modeling tools require information about the strain rates behavior of materials in terms of constitutive laws in a large range of strain rates. The experimental research developed by the

DynaMat laboratory of the University of Applied Sciences of Southern Switzerland in collaboration with Agrati Group, is inserted in this frame. The paper describes experimental techniques used to carry out dynamic tensile tests on steels used in fastening. The high strain rate tests have been performed using a JRC-Modified Hopkinson Bar (JRC-MHB) and a Split Hopkinson Pressure Bar (SHPB), while the medium strain rate tests have been performed by means of a Hydro-Pneumatic Machine (HPM). The tests have been carried out loading the specimens with tensile stress at different strain rates, from 5 to 2500 1/s.

The analysis of the material has been carried out studying both the experimental results in terms of engineering and true stress versus strain curves and fracture. The characteristics of fracture, the reduction of area of the specimen cross-section after failure in the necking zone, as well as the fracture strain, have been obtained by means of acquisition of two images, before and after the failure of the specimen. The tests have been also filmed utilizing a high speed camera in order to obtain information about the progression of the necking phase.

The higher strain rate tests have been carried out in the Laboratory of Dynamic Investigation of Materials in Nizhny Novgorod, in the frame of the Swiss – Russian Joint Research Program.

1.1. Manufacturing process

The production of a bolt for fastening is a quite complex process including wire/rod preparation, cold, warm or hot forming and thread rolling. A typical rod preparation cycle consists in: annealing of steel coils (spheroidizing); pickling in H_2SO_4; phosphating; cold drawing; storage before cold forming.

Fasteners are usually produced in multi-station forming machines, by cutting, heading and extrusion of the material, and thread rolling. The speed of these operations are rather high, in fact a multi-station forming machine is normally able to produce 60 to 200 pieces by minute, according to the fastener dimension and complexity.

After the forming process, the cycle usually includes heat treatment to give the defined mechanical properties, and the application of coating/lubrication on fasteners, to ensure performances in terms of corrosion resistance and friction coefficient. The result of a finite element analysis of the cold forming cycle is shown in Fig. 1. In this example, the total equivalent plastic strain is the selected parameter.

All four cold forming steps are shown in Fig. 2. The last but one is the result of thread rolling; and the last one in the picture is the bolt after heat treatment and after non-electrolytically applied zinc flake coating. Thread is obtained by plastic deformation of the shank, without any removal of the material.

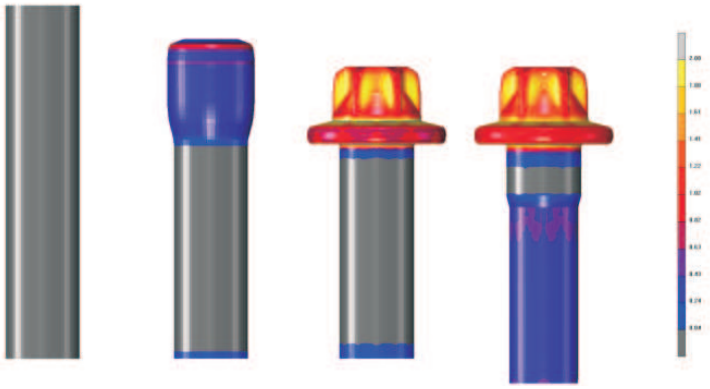

FIG. 1. FEM results of the cold forming cycle.

FIG. 2. Sequence of cold forming of fastener.

2. MATERIAL

The analyzed material is the 30MnB4 steel, according to EN 10263-4 [1]. The chemical composition of this steel is shown in Table 1.

Table 1. Chemical composition.

	C	Si	Mn	P	S	Cr	Mo	Cu	B
Standard Requirements	0.27÷0.32	≤ 0.30	0.80÷1.10	≤ 0.025	≤ 0.025	≤ 0.30	–	≤ 0.25	0.0008÷0.005
Specimens	0.28	0.12	0.83	0.01	0.004	0.17	–	0.13	0.0027

The steel was supplied by the steelmaker in hot-rolled condition, with rod diameter of 7.50 mm. The material is normally characterized by a tensile strength $R_m = 632 \div 640$ MPa and the percentage reduction of area after fracture $Z = 62 \div 50\%$.

In this case, after the preparation cycle, the rod for specimens has got the following characteristics:

- diameter = 6.15 mm (reduction of area during cold drawing $\approx 33\%$);
- tensile strength $R_m = 695 \div 720$ MPa;
- percentage reduction of area after fracture $Z = 55 \div 59\%$;
- core hardness ≈ 238 $HV_{0.3}$.

The micro-hardness scanning (Fig. 3) shows superimposed effects of hot rolling, annealing and cold drawing processes of the rod.

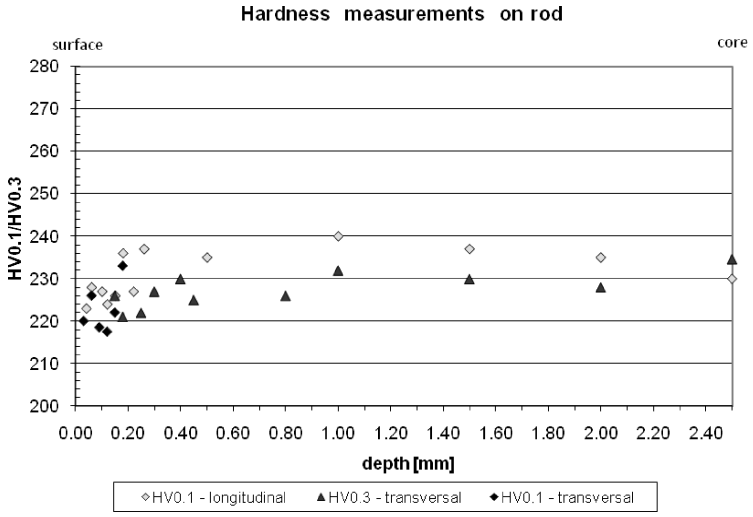

FIG. 3. Hardness distribution on the depth.

To discuss micro-hardness profiles it is important to take into consideration the residual stresses distribution, whose effects are to be added to the grain dimensions.

In Fig. 4a and Fig. 4b the transversal and the longitudinal section in the core are shown (500×). In the first picture it is possible to observe the not completely

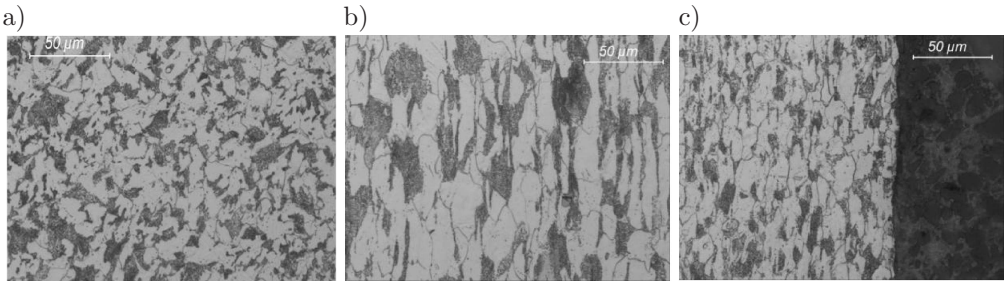

FIG. 4. Ferritic-pearlitic micro-structure.

lamellar pearlite and in the second picture – the longitudinal "pancaked" grain. Finally, in Fig. 4c, the longitudinal section at the surface (500×) is shown, where the grain refinement compared to the core micro-structure is evident.

3. Experimental program

The experimental techniques for high-strain-rate measurements are described in literature [2–7]. The dynamic tests were conducted on round specimens depicted in Fig. 5.

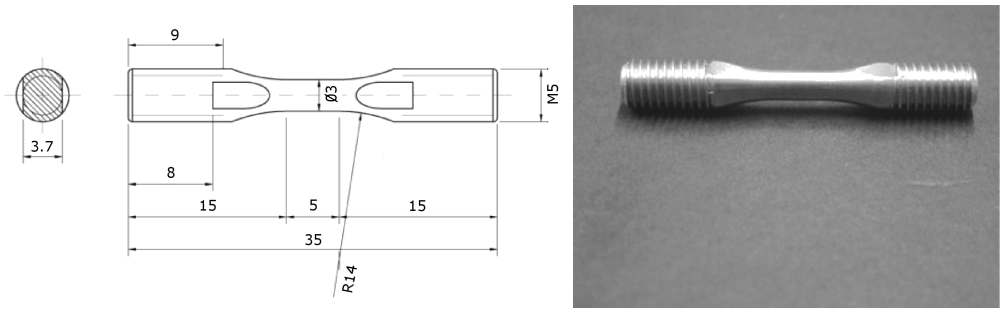

Fig. 5. Specimen geometry.

These specimens were tested in different conditions: using stroke-controlled static procedures and with HPM, JRC-MHB and SHPB dynamic experimental techniques. The Universal Machine used for quasi-static tests and the HPM used for medium strain rates are shown in Fig. 6.

a) b)

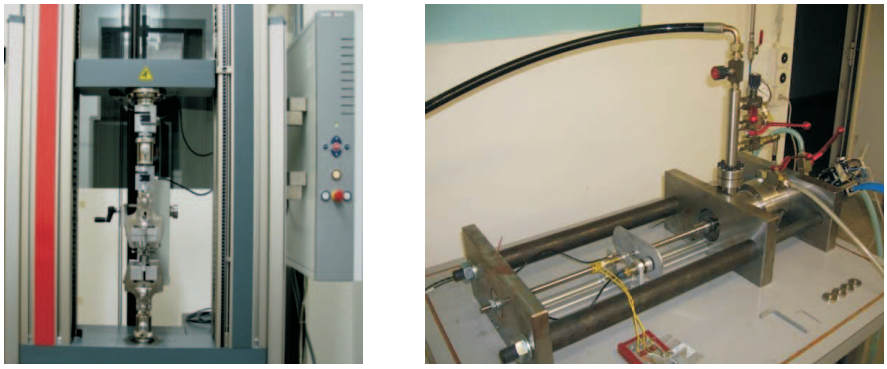

Fig. 6. a) Universal Machine; b) Hydro-Pneumatic Machine.

The JRC-MHB has been used for high strain-rate tests and consists of two cylindrical high strength steel bars, having a diameter of 10 mm, with length

of respectively 9 and 6 m for the input and output bar. The steel specimen is assembled between the two bars, as shown in Fig. 7 [8–9].

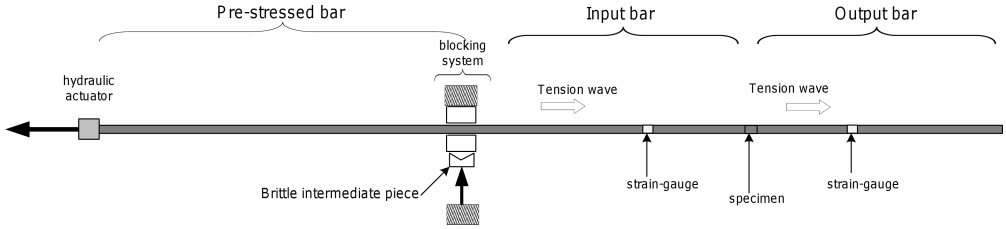

FIG. 7. JRC-MHB scheme.

The test with the MHB is performed as follows:

1) an hydraulic actuator, with maximum loading capacity of 600 kN, applies a tensile load on a part of the input bar (pre-stressed bar, with a length of 6 m and diameter of 10 mm); a blocking device permits to store elastic energy pulling the pre-tension bar;
2) breaking of the brittle bolt in the blocking device gives rise to a tensile mechanical pulse, which propagates along the input and output bars and brings the specimen to fracture. The pulse has a duration of 2.4 ms, with linear loading rate rise time of 30 μs.

The input and output bars are instrumented with strain gauges which measure the incident, reflected and transmitted pulses acting on the cross-section of the specimen. A part of the input bar is used as a pre-stressed bar. On the basis of the incident (ε_I), reflected (ε_R) and transmitted (ε_T) records, of the consideration of the basic constitutive equation of the input and output elastic bar material, of the one-dimensional wave propagation theory, it is possible to calculate the stress, strain and strain-rate curves with the following equations [10–12]:

$$\sigma_E(t) = E_0 \frac{A_0}{A} \varepsilon_T(t), \qquad \varepsilon_E(t) = -\frac{2C_0}{L} \int_0^t \varepsilon_R(t)dt, \qquad \dot{\varepsilon}(t) = -\frac{2C_0}{L} \varepsilon_R(t), \tag{3.1}$$

where E_0 is the elastic modulus of the bars; A_0 is their cross-section area; A is the specimen cross-section area; L is the specimen gauge length; C_0 is the sound velocity of the bar material.

Similar tests have been carried out using a traditional SHPB (Fig. 8) placed in the Nizhny Novgorod State University [13]. Pulse loads in a SHPB are generated using compact 10-mm gas guns. Tensile tests are conducted following the modified Nicholas scheme [14]. For testing high-strength steel, pressure bars of 12 mm diameter were used. The first pressure bar is 1.5 m long and the second

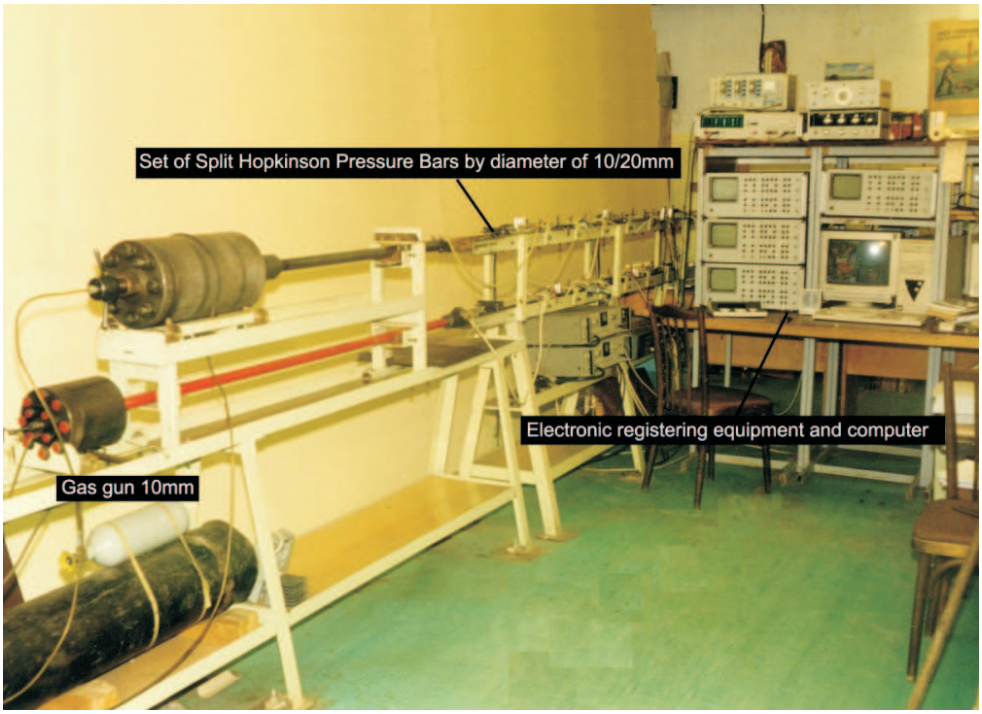

FIG. 8. SHPB for dynamic tests.

bar that has a free rear end is 0.75 m long. Tensile pulse in the Nicholas' scheme is formed due to the presence of a split ring surrounding the specimen (Fig. 9) and reflection of the transmitted pulse from the free rear end of the second bar.

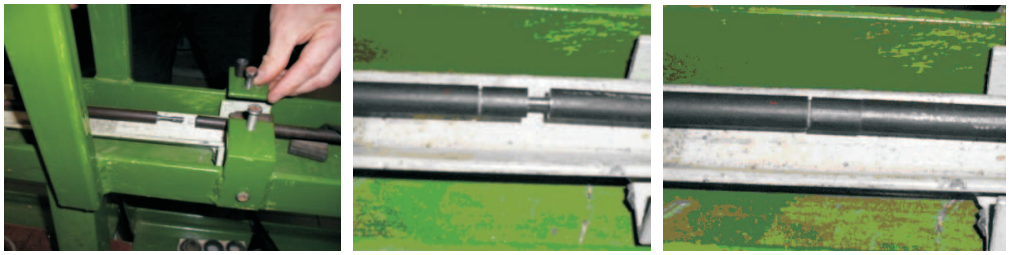

FIG. 9. Phases of the assembly of the specimen to the testing device.

4. Results and discussion

The results of the preliminary tests are collected in Table 2. In Fig. 10 the engineering and true stress versus strain are depicted.

a)

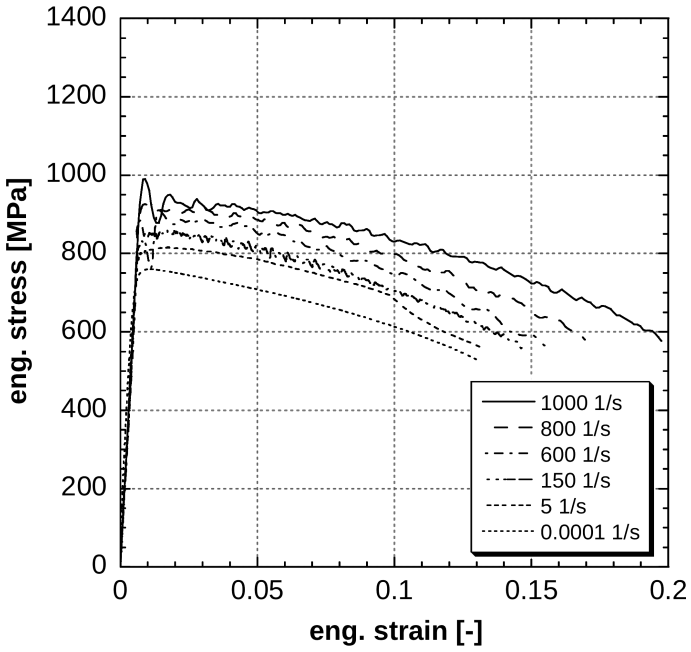

b)

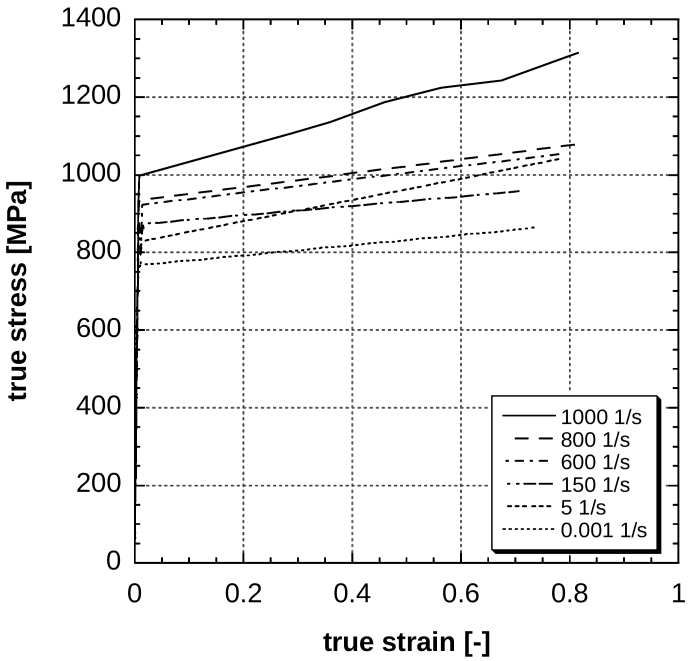

FIG. 10. a) engineering stress vs. engineering strain curves; b) true stress vs. true strain curves.

Table 2. Experimental results.

Strain rate [s^{-1}]	R_m [MPa]	Uniform elongation ε_u	Total elongation ε_t	Reduction of area Z [%]
10^{-3}	770	1.2%	13.1 %	52.3
5	815	1.7%	13.2%	52.4
150	856	1.7%	14.6%	50.6
600	899	1.4%	15.5%	54.5
800	926	1.0%	16.9%	55.7
1000	990	0.9%	19.7%	55.7

In order to analyze the failure behavior of 30MnB4 steel, some tests have been recorded by a Specialized Imaging Duplex Ultra Fast Framing Camera (with a speed up to 200 Mfps, see Fig. 11b), able to record up to 16 images without compromising on shading, or parallaxing. In Fig. 11a is shown the engineering stress versus strain curves, with the indication of the photo made by the fast camera.

The photos of the failure (Fig. 11c-h) reveal the ability of the camera to capture the necking process.

The true stress vs. true strain curve is regarded as significant until the ultimate tensile stress (where the necking begins) is reached. After this point, stress localization and fracture propagation governs the flow curve, which is no more representative for homogeneous mechanical properties of the materials. In this case, beyond the point of ultimate strength in the engineering stress-strain curve, the one-dimensional true stress-strain curve should be reconstructed, by calculating the true stress and the true strain using the Bridgman formulae, [15] which introduces the correction for the triaxial stress state. At fracture the Bridgman formulae can be written as follows:

$$\sigma_{\text{true,fracture}} = \frac{\sigma_{\text{eng.,fracture}}}{(1 + 2R/a) \cdot \ln(1 + a/2R)}, \tag{4.1}$$

where a – minimum radius at fracture cross-section, R – meridional profile radius at fracture neck (see Fig. 13a), $\sigma_{\text{true,fracture}} = P_{\text{fracture}}/\pi a^2$ – the average true stress at fracture and P_{fracture} the fracture force.

$$\varepsilon_{\text{true,fracture}} = 2 \cdot \ln \frac{a_0}{2 \cdot a}, \tag{4.2}$$

where a_0 is the initial diameter of the gauge length cross-section.

For the complete construction of the true stress-strain curve during the necking deformation phase, a straight line is drawn between the ultimate tensile strength (uniform strain) point and the fracture point, the latter being determined by application of Eqs. (4.1) and (4.2).

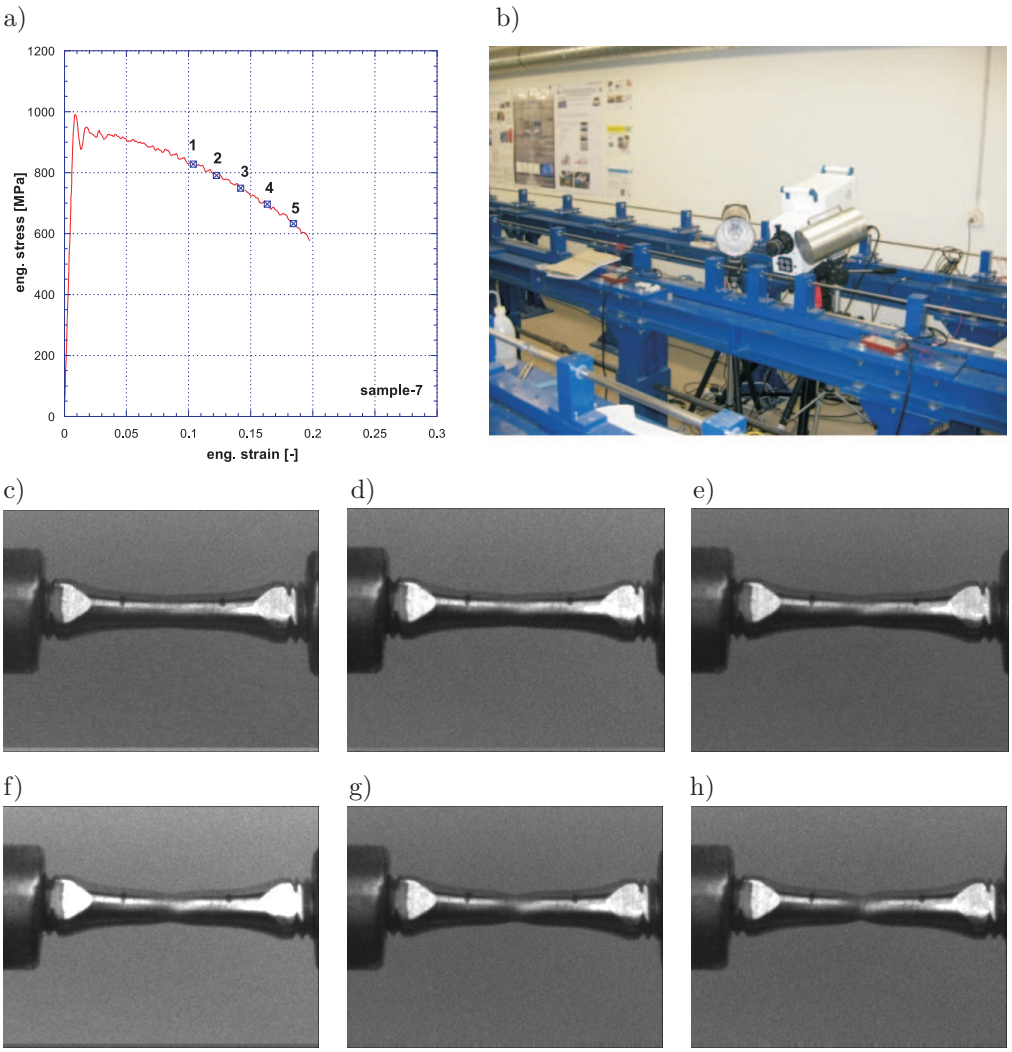

FIG. 11. High speed digital camera.

A more refined determination of the true stress vs. true strain curve between the point of ultimate tensile strength (uniform strain) and the point of fracture, has been performed, using the following method:

- fast recording of the test,
- repetition, at defined increasing deformation levels, of the optical measurements of the meridional radius at neck (R) and of the minimum radius at neck cross-section (a),
- calculation, with the Eqs. (4.1) and (4.2), of the true stress and true strain values, for the defined deformation levels.

In Fig. 12b the results of the described measurement are shown. It is possible to observe how well the linear trend describes the necking process in the true stress vs. true strain diagram. Subsequently we have demonstrated a good approximation of the procedure which only exploits the Bridgman formulae and the information given by the engineering curve, and by the measurement of the fracture geometry.

a)

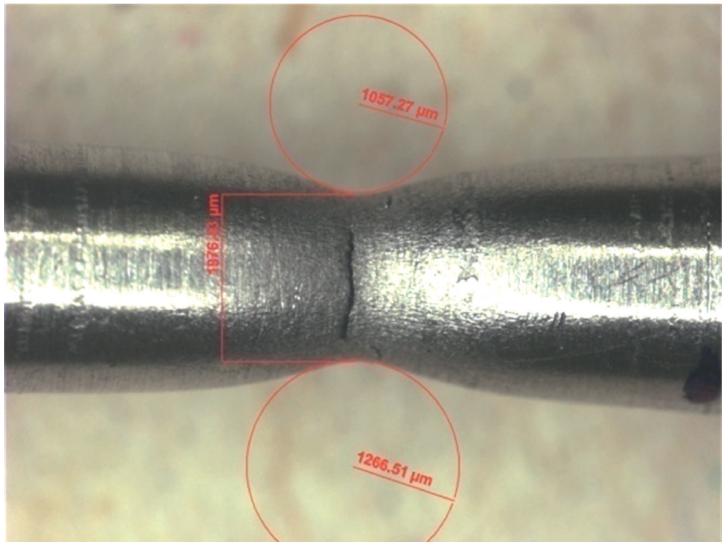

b)

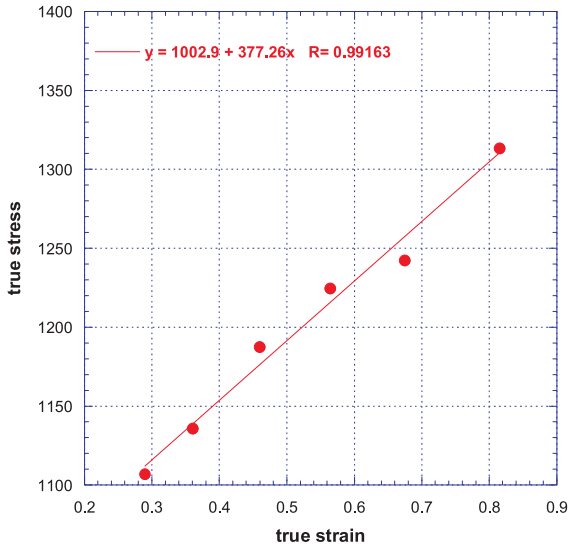

FIG. 12. a) parameter for Bridgman formulae; b) points measured by fast camera.

4.1. Comparison between JRC-MHB and SHPB

The SHPB is not able to generate enough energy to break the specimen for strain rates less than 1000 1/s because of the short length of the striker bar. The comparison of two tests performed with SHPB and JRC-MHB is shown in Fig. 13a; in the first case, the specimen is only deformed to the necking phase (see Fig. 13b) while in the JRC-MHB all the plastic fields are detected, till failure. At the moment, the JRC-MHB set up does not reach the same velocities of the SHPB. To obtain those values, the JRC-MHB should be realized in very high strength material (for instance a thermally aged, maraging steel), instead of the high strength steel actually utilized. In order to obtain low strain rate with the SHPB, longer striker bar should be adopted.

a) b)

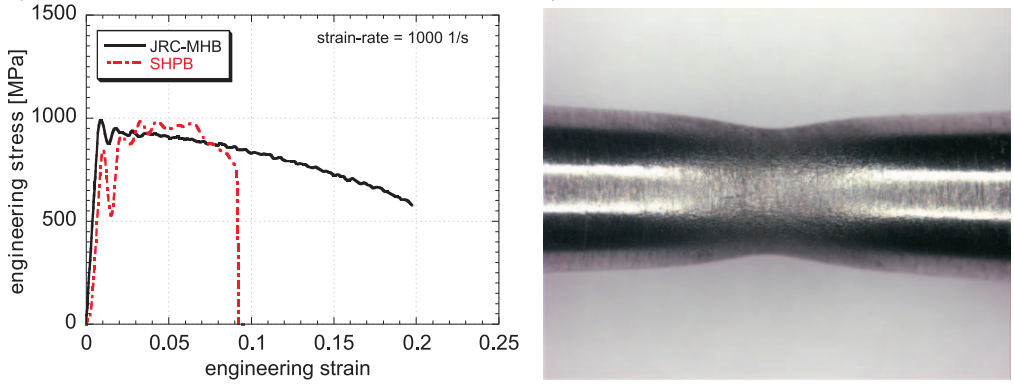

FIG. 13. a) Comparison of the two test set-ups; b) Necking in the specimen.

During the testing activities, the influence of the rise time of the load process on the materials behavior, in the elastic range, has been noted. This phenomenon, observed for HSS steels, is evidenced as an instability of the curves, which shows a high first peak. The rise time of the SHPB set-up is about 150 μs, while the JRC-MHB set-up reaches up to 30 μs.

For the tensile tests in particular, the JRC-MHB set-up permits to obtain a perfect direct loading of the specimen, while in the SHPB set-up this is obtained by inversion of the waves at the free end of the bar. The comparison between the records observed within the two solutions is shown in Fig. 14.

Specimens at high strain rates, over 1000 1/s, have been tested with the SHPB apparatus.

Three true stress curves versus true strain curves are depicted in Fig. 15a. The increase of the ultimate tensile strength in function of the logarithm of the strain rate is shown in Fig. 15b. Up to 1000 1/s, the Dynamic Increase Factor is less than 1.2; for higher true strain values the DIF could be more than 1.8.

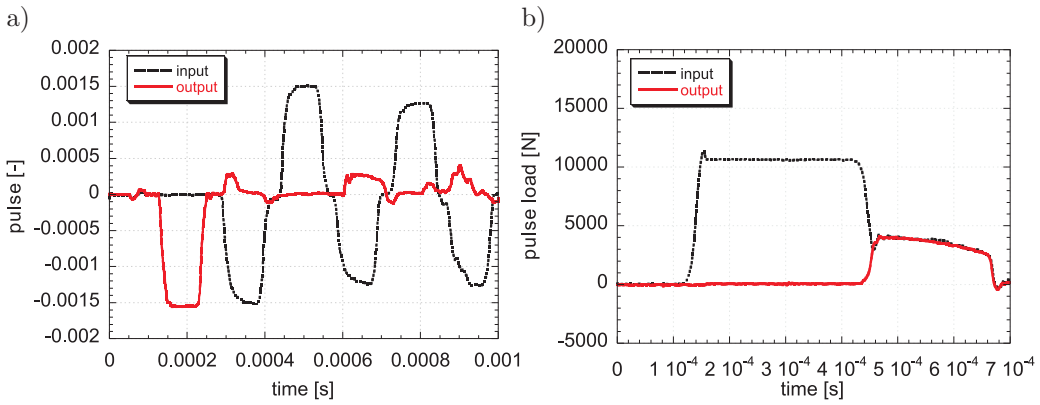

FIG. 14. Signals from: a) SHPB; b) JRC-MHB.

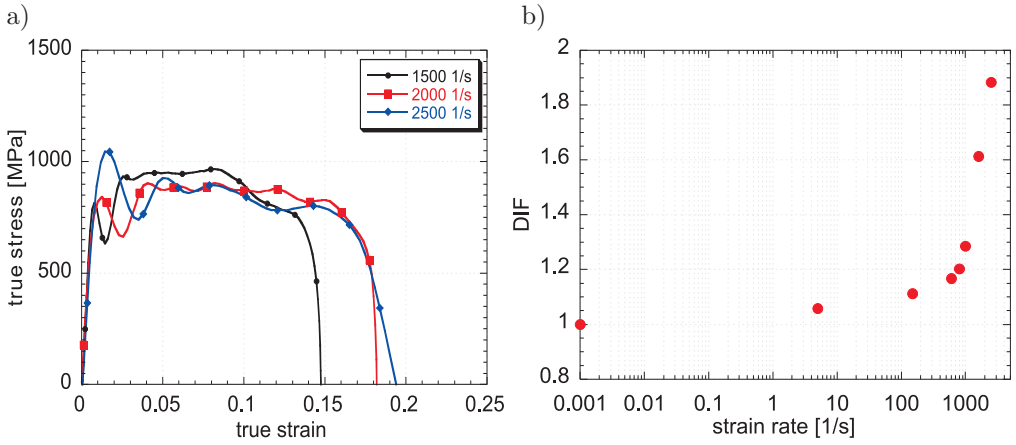

FIG. 15. a) high strain rate tests with SHPB; b) Dynamic Increase Factor (DIF) versus strain rate.

5. Example of a material constitutive law calibration

Advanced modeling tools require information about the strain rate behavior of materials in terms of constitutive laws in a large range of strain rates. Also in the case of fasteners this topic cannot be avoided. In this paragraph the plastic behavior of the 30MnB4 steel by the Johnson-Cook constitutive model [16] is explained. This model is intensively used to describe the material strength in the numerical simulations of dynamic events and provides satisfactory results, when strain rates are lower than 10^3 s^{-1}. This model assumes that the dependence of the stress on the strain, strain rate and temperature can be multiplicatively

decomposed into three separate functions. Then, this model gives the following relation for the flow stress σ_0:

$$\sigma_0 = [A + B \cdot (\epsilon_p)^n] \cdot \left[1 + C \cdot \ln\left(\frac{\dot{\epsilon}_p}{\dot{\epsilon}_0}\right)\right] \cdot [1 - T^{*m}], \tag{5.1}$$

where ϵ_p is the equivalent plastic strain, $\dot{\epsilon}_p$ is the considered test strain rate, $\dot{\epsilon}_0$ is a reference strain rate (usually equal to 1 s^{-1}), A, B, C, n and m are five material constants that have to be determined. The parameter n takes into account the strain hardening effect, the parameter m models the thermal softening, and C represents the strain rate sensitivity. Finally T^* is:

$$T^* = \begin{cases} 0 & \text{for} \quad T \leq T_r, \\ \dfrac{T - T_r}{T_m - T_r} & \text{for} \quad T_r < T \leq T_m, \\ 1 & \text{for} \quad T > T_m, \end{cases} \tag{5.2}$$

where T is the current temperature, T_m is the melting temperature (assumed 1507°C for the 30MnB4 steel), and T_r is a reference temperature.

5.1. Determination of A, B and n in the JC model

The experimental quasi-static data can be used to plot the plastic curve characteristic of the material at room temperature (20°C): σ_{true} versus ϵ_p. This curve is best fitted by:

$$\sigma_0 = A + B \cdot \epsilon_p^n, \tag{5.3}$$

where $A = 625$ MPa is the stress yield point of the static curve, while B and n are determined using a regression-analysis procedure. The obtained parameters are $B = 628.9$ MPa and $n = 0.4097$ (with $R^2 = 0.7672$).

5.2. Determination of C in the JC model

Firstly, it is assumed that the reference strain rate is $\dot{\epsilon}_0 = 1$ s^{-1}. It is further assumed that the specimen remains at room temperature, thus neglecting the thermo-plastic effects ($T^8 = 0$). Assuming that the strain rate is constant during the experiment, the parameter C is evaluated for three different strain rates ($\dot{\epsilon}_p$): 5 s^{-1}, 135 s^{-1} and 611 s^{-1}.

Under these assumptions the experimental stress versus plastic strain curves were fitted with the following formula:

$$\sigma_0 = [625 + 628.9 \cdot (\epsilon_p)^{0.4097}] \cdot \left[1 + C \cdot \ln\left(\frac{\dot{\epsilon}_p}{\dot{\epsilon}_0}\right)\right]. \tag{5.4}$$

5.3. *Determination of in the JC model*

In order to determine the parameter m, experimental results at both the room temperature and higher temperature are needed. Experimental results at high strain rates at 20°C and 450°C have been used.

The ratio R between the stresses at a specific plastic strain can be calculated if experiments at the same strain rate are carried out. In particular, m can be evaluated as:

$$m = \frac{\log(1-R)}{\log(T^*)}. \tag{5.5}$$

Considering the true stresses at the temperature 450°C divided by the true stresses at room temperature (20°C), in the flow true stress versus plastic strain curve, it results an average value of $R = 0.6031$. Substituting this value into Eq. (5.5), $m = 0.7448$ is obtained.

The results of the calculated parameters are reported by the following table. Figure 16 shows the goodness of the Johnson-Cook fit up to 10 1/s. For higher values of strain rates it seems that this relationship does not appropriately describe the real behavior of the material; for this reason, our attention will be focused to the development of future new constitutive laws.

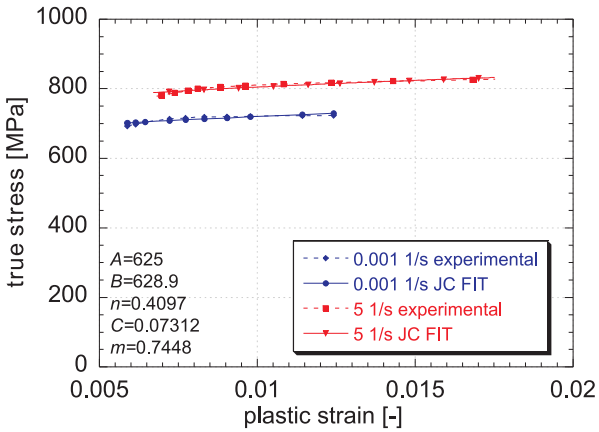

FIG. 16. Experimental data vs. JC FIT for 30MnB4 at 5 s^{-1}.

6. CONCLUDING REMARKS

The 30MnB4 steel tested in this preliminary phase resulted to be rate sensitive. This steel is usually adopted for fasteners. The manufactory process induces into the material a very complicated history of strain, provoked by cold forming and thread rolling. The production procedure is often carried out at a high

velocity, then a mechanical characterization in a wide range of strain rates is needed.

In this preliminary phase a series of tests by means of different experimental techniques have been performed, in order to show the capability of describing the actual material behavior.

It has been demonstrated how the fast recording of the failure process is well described by a linear function between the ultimate tensile strength/uniform strain, the failure point obtained by the Bridgman formulae and the geometric information by the high speed digital camera.

The high strain rate behavior has been studied by means of two types of set-ups. The traditional SHPB and the JRC-MHB have been compared. From this comparison, some comments can be summarized. First of all, the capacity of the JRC-MHB to follow the full plastic field in the range of strain rates between 100 and 1000 1/s, in the case of traditional SHPB, this is not possible without the use of longer striker bar. The JRC-MHB performs direct tensile test; the same cannot be affirmed for the SHPB. In fact, it uses the reflected wave from the free end but the presence of spurious reflection, due to the split ring, causes overlapping waves what is often difficult to analyze. The SHPB should be used in compression; to obtain direct tensile test, the pulse should be directly applied.

An example of calibration of the Johnson-Cook model has been carried out, in order to integrate the results in numerical codes and to reproduce plastic deformation occurring in dynamic regime for 30MnB4 steel.

These results indicate the advantage of using a dynamic characterization of steel, in order to improve the quality of the fastener products and enhance the production capacity.

Acknowledgements

The Authors are grateful to Mr. Wai Chan and Mr. Peter Berkenberg from "Specialised Imaging" for their precious collaboration in the execution of high speed measurements. A special acknowledgement goes to the Scientific & Technological Cooperation Programme Switzerland-Russia for the financial support of the Utilization of Specific Infrastructure Projects called "Dynamic behaviour of materials for industrial applications". Russian part of investigations was partially financed by RFBR (grant 10-01-00585).

References

1. EN 10263-4: 2003. "Steel rod, bars and wire for cold heading and cold extrusion. Part 4: technical delivery conditions for steels for quenching and tempering".
2. M. A. Meyers, *Dynamic Behavior of Materials*, Wiley Interscience, New York, 1994.

3. J. E. Field, *Review of experimental techniques for high rate deformation and shock studies*, Int. J. Imp. Eng., **30**, 725–775, 2004.

4. G. T. Gray III, *Classic Split-Hopkinson pressure bar testing*, [in:] ASM Handbook, Vol. 8, H. Kuhn, D. Medlin [Eds.], ASM Int., Materials Park Ohio 2000, pp. 462–476.

5. K. A. Hartley, J. Duffy, R. H. Hawley, *The torsional Kolsky (Split-Hopkinson) bar*, [in:] ASM Handbook, Vol. 8, H. Kuhn, D. Medlin [Eds.], ASM Int., Materials Park Ohio 1985, pp. 218–228.

6. S. Vaynman, M. E. Fine, S. Leeb, H. D. Espinosa, *Effect of strain rate and temperature on mechanical properties and fracture mode of high strength precipitation hardened ferritic steels*, Scripta Materialia, **55**, 351–354, 2006.

7. T. Nicholas, A. M. Rajendran, *Material characterization at high strain-rates*, [in:] High Velocity Impact Dynamics, J.A. Zukas [Ed.], Wiley, New York 1990, pp. 127–296.

8. C. Albertini, M. Montagnani, *Testing techniques based on the split Hopkinson bar*, Institute of Physics Conference series No. 21, pp. 22–32, London, 1974.

9. C. Albertini, M. Montagnani, *Waves propagation effects on dynamic loading*, Journal NED 37, pp. 115–124, North Holland Publishing Company, 1976.

10. R. M. Davis, *A critical study of the Hopkinson bar*, Cambridge University Press, **240**, 375–457, 1948.

11. H. Kolsky, *An investigation of the mechanical properties of materials at very high rates of loading*, Proc. Phys. Soc. Sect. **B62**, 676–700, 1949.

12. U. S. Lindholm, *High strain rate tests*, Techniques of metal research, J. Wiley [Ed.], **5**, 1, 1971.

13. A. M. Bragov, P. V. Demenko, A. K. Lomunov, I. V. Sergeichev, L. Kruszka, *Investigation of behaviour of materials of different physical nature using the Kolsky method and its modifications*, New Experimental Methods in Material Dynamics and Impact, Trends in Mechanics of Materials, W.K. Nowacki, J.R. Klepaczko [Eds.], Warsaw, 2001, pp. 337–348.

14. T. Nicholas, *Tensile testing of materials at high rates of strain*, Exp. Mech., **21**, 5, 177–195, 1981.

15. P. W. Bridgman, *Studies in large plastic flow and fracture*, Mc Graw-Hill, 1952.

16. G. J. Johnson, W. H. Cook, *A constitutive model and data for metals subjected to large strains, high strain rates and high temperatures*, Proceedings of the Seventh International Symposium on Ballistics, The Hague, 1983, pp. 541–547.

Received January 11, 2011; revised version June 4, 2011.

ENGINEERING TRANSACTIONS • *Engng. Trans.* • **59**, 2, 119–136, 2011
Polish Academy of Sciences • Institute of Fundamental Technological Research (IPPT PAN)
National Engineering School of Metz (ENIM)

SOME REMARKS ON BURZYŃSKI'S FAILURE CRITERION FOR ANISOTROPIC MATERIALS

P. Szeptyński

AGH University of Science and Technology
Faculty of Mechanical Engineering and Robotics
Department of the Strength and Fatigue of Materials and Structures
Kraków, Poland
e-mail: pszept@agh.edu.pl

Some misstatements appearing in the final form of the failure criterion formulation, derived from Burzyński's hypothesis of material effort for anisotropic bodies, which haven't been noticed in the literature as yet, are pointed out and discussed. Alternative interpretations of the results obtained by Burzyński are presented. Propositions of different formulation of the failure criterion, basing on original ideas of Burzyński, are given.

Key words: Burzyński's hypothesis, limit condition, material effort, anisotropy.

1. Introduction

Among many propositions of the hypotheses of material effort for isotropic bodies, the one proposed by Burzyński in his doctoral dissertation (1928 [1]), surprises by its clear energy-based interpretation, variety of classes of materials it can be applied to and simplicity in formulation of the failure criterion, which can be determined only in terms of limit stresses under simple loads: uniaxial tension, compression and pure shear. Accounting for pressure sensitivity, Burzyński developed former ideas of his teacher, M.T. Huber [2], and anticipated later propositions of Drucker and Prager [3]. From the late twenties of the 20th century until now it remains one of the most general and practical propositions stated. However, it seems to be still underestimated, almost forgotten, especially abroad Poland. Extension of the given hypothesis accounting for anisotropy is even less known despite the fact that it was something completely new at that time – it could be compared only with some ideas introduced in the same year by Mises [4]. Both papers were published a few decades before other similar propositions by Hill (1948 [5]) or Hoffman (1967 [6]). Small popularity of the anisotropic version of Burzyński's condition is the reason for which it was not discussed as yet. In the current paper, some misstatements

in the formulation given by Burzyński, which were not noticed and discussed in the literature, are pointed out. It is also the aim of the author to suggest alternative interpretation of the results obtained by Burzyński and to propose a formulation of the final limit condition, derived from Burzyński's hypothesis of material effort different from the original one.

2. Burzyński's hypothesis of material effort for anisotropic bodies

Burzyński considered an energy-based failure criterion, in which elastic energy density is expressed assuming linear dependence between the stress and strain states:

$$\begin{aligned} \mathbf{C}\boldsymbol{\sigma} = \boldsymbol{\varepsilon} \quad &\Rightarrow \quad C_{ijkl}\sigma_{kl} = \varepsilon_{ij}, \\ \mathbf{S}\boldsymbol{\varepsilon} = \boldsymbol{\sigma} \quad &\Rightarrow \quad S_{ijkl}\varepsilon_{kl} = \sigma_{ij}, \end{aligned} \tag{2.1}$$

where $\mathbf{C}$ and $\mathbf{S}$ are fourth order symmetric compliance and stiffness tensor respectively, $\boldsymbol{\sigma}$ is the stress tensor and $\boldsymbol{\varepsilon}$ is an infinitesimal strain tensor. Assumption that Hooke's law is still valid even just before reaching the limit state, indicates that the limit state considered by Burzyński is in fact the limit of Hooke's law validity range – linear elasticity. All the limit stress quantities appearing in this formulation should be considered as the proportionality limit.

2.1. Hypothesis statement

Burzyński proposed to consider as a measure of material effort, the combination of distortional strain energy density and a part of volume change energy density, determined by function η, namely:

$$\Phi_f + \eta \cdot \Phi_v = K, \tag{2.2}$$

where K – limit value of energy density,

$$\Phi_v = \frac{1}{2}\mathbf{A}_\sigma \cdot \mathbf{A}_\varepsilon = \frac{1}{2}\left(\frac{1}{3}\mathrm{tr}(\boldsymbol{\sigma})\mathbf{1}\right) \cdot \left(\frac{1}{3}\mathrm{tr}(\boldsymbol{\varepsilon})\mathbf{1}\right),$$

$$\Phi_f = \frac{1}{2}\mathbf{D}_\sigma \cdot \mathbf{D}_\varepsilon = \frac{1}{2}\left(\boldsymbol{\sigma} - \frac{1}{3}\mathrm{tr}(\boldsymbol{\sigma})\mathbf{1}\right) \cdot \left(\boldsymbol{\varepsilon} - \frac{1}{3}\mathrm{tr}(\boldsymbol{\varepsilon})\mathbf{1}\right),$$

$$\eta = \eta(p, \delta, \omega) = \left(\omega + \frac{\delta}{3p}\right).$$

$\mathbf{A}_\sigma$, $\mathbf{A}_\varepsilon$ and $\mathbf{D}_\sigma$, $\mathbf{D}_\varepsilon$ are spherical parts and deviators of stress and strain tensors respectively, $\mathbf{1}$ is an isotropic second rank symmetric tensor (identity tensor),

p denotes hydrostatic stress, and δ and ω are constant material parameters. The form of the function η was assumed by Burzyński.

Decomposition of the strain energy density into distortional and volumetric strain energy density is possible in general only for isotropic bodies or those of cubic symmetry. However, Burzyński stated that: *'Practically there are no physical reasons for which strain energy could not be decomposed into sum of two other energies, namely volumetric strain energy and distortional strain energy'* [1]. He considered a special class of materials of arbitrary symmetry, which the considered decomposition is always possible or equivalently – speaking in terms of tensor algebra – for which hydrostatic stress and dilatation are eigenstates of compliance and stiffness tensor respectively [7]:

$$\mathbf{C1} = \Theta\mathbf{1} \quad \Rightarrow \quad C_{ijkl}\delta_{kl} = \Theta\delta_{ij} \quad \Rightarrow \quad C_{ijkk} = \Theta\delta_{ij}, \tag{2.3}$$

where Θ is the proportionality coefficient (eigenvalue of $\mathbf{C}$). This assumption leads to the following constraints on the components of compliance/stiffness tensor:

$$\begin{aligned} &\text{(3 independent relations)} \begin{cases} C_{1123} + C_{2223} + C_{3323} = 0, \\ C_{1131} + C_{2231} + C_{3331} = 0, \\ C_{1112} + C_{2212} + C_{3312} = 0, \end{cases} \\ &\text{(2 independent relations)} \begin{cases} C_{1111} - C_{2222} = C_{2233} - C_{1133}, \\ C_{2222} - C_{3333} = C_{3311} - C_{2211}, \\ C_{3333} - C_{1111} = C_{1122} - C_{3322}. \end{cases} \end{aligned} \tag{2.4}$$

These equations are called the *Burzyński's conditions*. If components of compliance or stiffness tensor of a given material satisfy the Burzyński's conditions (2.4), it is called the *volumetrically isotropic* material or simply the *Burzyński's material*. Total number of independent components of stiffness or compliance tensor, in case of volumetric isotropy, is reduced from 21 to 16.

2.2. Limit conditions

In case of isotropy, after substituting:

$$\begin{aligned} \frac{1-2\mu}{1+\mu}\omega &= \frac{1-2\nu}{1+\nu}, & \frac{1-2\mu}{1+\mu}\delta &= \frac{3(k_c-k_r)}{1+\nu}, \\ 12GK &= \frac{3k_ck_r}{1+\nu}, & \nu &= \frac{k_ck_r}{2k_s^2} - 1, \end{aligned} \tag{2.5}$$

where G – Kirchhoff's modulus, μ – Poisson's ratio, k_c, k_r, k_s – limit values of stress at compression, tension and shearing tests, the general formulation of the

Burzyński hypothesis (2.2) can be expressed in terms of limit quantities, which are relatively easy to be measured:

$$\sigma_{11}^2+\sigma_{22}^2+\sigma_{33}^2+2\left(1-\frac{k_ck_r}{2k_s^2}\right)(\sigma_{22}\sigma_{33}+\sigma_{33}\sigma_{11}+\sigma_{11}\sigma_{22}) + \left(\frac{k_ck_r}{k_s^2}\right)(\sigma_{23}^2+\sigma_{31}^2+\sigma_{12}^2)+(k_c-k_r)(\sigma_{11}+\sigma_{22}+\sigma_{33})-k_ck_r=0. \tag{2.6}$$

As it was said before, Burzyński also made an attempt to account for anisotropy in his hypothesis knowing that in fact, there are no ideally isotropic materials. He has considered a fully anisotropic material (except of its volumetric isotropy), yet for simplification of the criterion formulation he reduced the number of independent parameters. He used the so-called '*basic*' (or '*fundamental*') coordinate system, in which in expression of elastic energy density, the mixed terms involving shearing and normal stresses (or equivalently, linear and distortional strains) vanish. After certain rotation – which is 'only mathematically possible' [1] for volumetrically isotropic bodies – of a given coordinate system to the position, in which it can be considered as the 'basic' one, even in case of very low symmetries (total anisotropy, monoclinic symmetry, trigonal symmetry), the expression of the elastic energy density has the mathematical form at least as simple as in case of orthotropy. Such situation occurs when the Burzyński's conditions (2.4) are fulfilled and additionally, the following relations are true:

$$\begin{aligned} C_{2223}\sigma_{23}-C_{1131}\sigma_{31}&=0,\\ C_{3331}\sigma_{31}-C_{2212}\sigma_{12}&=0,\\ C_{1112}\sigma_{12}-C_{3323}\sigma_{23}&=0. \end{aligned} \tag{2.7}$$

One can note that those conditions are fulfilled in case of a coordinate system with axes which are parallel to the directions of principal stresses, in which off-diagonal components of the stress tensor are always equal to 0. This is a very specific case – in fact there exist other basic coordinate systems, independent of the stress state. For example, in case of any material which is at least orthotropic (orthotropic, tetragonal, cylindrical, cubic), a coordinate system built on the axes of symmetry of such a material satisfies those conditions. In the basic coordinate system, elastic energy density can be expressed as follows:

$$\Phi=\underbrace{\frac{1}{2}B(\sigma_{11}+\sigma_{22}+\sigma_{33})^2}_{\Phi_v} + \underbrace{\frac{1}{3}\left[L(\sigma_{22}-\sigma_{33})^2+M(\sigma_{33}-\sigma_{11})^2+N(\sigma_{11}-\sigma_{22})^2\right]+2P\sigma_{23}^2+2Q\sigma_{31}^2+2R\sigma_{12}^2}_{\Phi_f}, \tag{2.8}$$

where

$$
\begin{aligned}
B &= \frac{1}{3}(C_{kk11} + C_{kk22} + C_{kk33}) \\
&\quad = \frac{1}{3}(C_{11kk} + C_{22kk} + C_{33kk}), \quad k = 1,2,3 \quad \text{(no summation)}, \\
L &= \frac{3}{2}(B - C_{2233}), \\
M &= \frac{3}{2}(B - C_{3311}), \\
N &= \frac{3}{2}(B - C_{1122}), \\
P &= \frac{1}{4}\left(C_{2323} + 2C_{2331}\frac{C_{2223}}{C_{1131}}\right), \\
Q &= \frac{1}{4}\left(C_{3131} + 2C_{3112}\frac{C_{3331}}{C_{2212}}\right), \\
R &= \frac{1}{4}\left(C_{1212} + 2C_{1223}\frac{C_{1112}}{C_{3323}}\right),
\end{aligned}
\tag{2.9}
$$

B – bulk modulus, L, M, N, P, Q, R – generalized moduli of distortion.

Using the above formula in criterion (2.2) would give us the limit condition depending on 8 parameters, what makes it rather complex in analysis. In order to simplify it, Burzyński considered the strain energy density expressed only in terms of principal stresses – yet, he based on the assumption that $\sigma_1 \geq \sigma_2 \geq \sigma_3$ (or a set of inverted inequalities), what in simple load cases (uniaxial tests, pure shears) always guarantees that $\sigma_2 = 0$. In such a case, after further substitutions:

$$
\begin{aligned}
\frac{1-2\widetilde{\nu}}{1+\widetilde{\nu}} &= \frac{3BM}{2LN}\omega, & \frac{3(k_c - k_r)}{1+\widetilde{\nu}} &= \frac{3BM}{2LN}\delta, \\
\frac{3k_c k_r}{1+\widetilde{\nu}} &= \frac{3KM}{LN}, & \lambda &= \frac{M^2}{2LN}, \\
\frac{M}{L} &= \frac{M}{N} = 2(1-\lambda), & \varphi &= \sqrt{\frac{2(1+\lambda)}{3}}, \\
\widetilde{\nu} &= \frac{1}{\varphi^2}\frac{k_c k_r}{2k_s^2} - 1, & \widetilde{\delta} &= \frac{1+\widetilde{\nu}}{3}(1-2\lambda),
\end{aligned}
\tag{2.10}
$$

hypothesis (2.2) for anisotropic bodies can be written as a 4-parameter limit criterion, i.e. as:

$$\sigma_1^2+\left(\frac{(1-2\lambda)k_ck_r}{2(\lambda+1)k_s^2}+1\right)\sigma_2^2+\sigma_3^2+(k_c-k_r)(\sigma_1+\sigma_2+\sigma_3)$$
$$+2\left(1-\frac{k_ck_r(2-\lambda)}{2(\lambda+1)k_s^2}\right)\left[\sigma_2\sigma_3+\frac{(k_ck_r-2k_s^2)(\lambda+1)}{k_ck_r(2-\lambda)-2(\lambda+1)k_s^2}\sigma_3\sigma_1+\sigma_1\sigma_2\right]-k_ck_r=0. \tag{2.11}$$

Please note that while the limit condition proposed by Burzyński for isotropic bodies [1] is a scalar function of the first invariant of stress tensor and the second invariant of its deviator, function (2.11) can be no longer expressed in terms of only those two quantities. Proposition (2.11) can be considered as an extension of the limit condition for isotropic bodies, so that it accounted for the influence of the third stress tensor invariant; in this case, Lode angle dependence would be a result of distinct influence of the intermediate stress on the material effort. The influence of the Lode angle which is proportional to the third invariant of the stress deviator, can be easily observed on the plots of limit surfaces (in the space of principal stresses) which are no longer axi-symmetric surfaces.

2.3. Matrix form of the Burzyński limit condition for anisotropic bodies

The above limit condition (2.11) can be rewritten in such a matrix form:

$$\begin{bmatrix}\sigma_1\\ \sigma_2\\ \sigma_3\end{bmatrix}^T\begin{bmatrix}1 & \beta & \gamma\\ & \alpha & \beta\\ \text{sym} & & 1\end{bmatrix}\begin{bmatrix}\sigma_1\\ \sigma_2\\ \sigma_3\end{bmatrix}+\begin{bmatrix}(k_c-k_r)\\ (k_c-k_r)\\ (k_c-k_r)\end{bmatrix}^T\begin{bmatrix}\sigma_1\\ \sigma_2\\ \sigma_3\end{bmatrix}-k_ck_r=0, \tag{2.12}$$

where

$$\alpha=1+\frac{(1-2\lambda)k_ck_r}{2(\lambda+1)k_s^2},\qquad \beta=1-\frac{(2-\lambda)k_ck_r}{2(\lambda+1)k_s^2},\qquad \gamma=1-\frac{k_ck_r}{2k_s^2}.$$

Spectral decomposition of a linear matrix operator (which could be considered as a kind of a limit state tensor in the space of principal stresses), gives us an interesting result:

- One-dimensional subspace of hydrostatic stresses:
  Eigenvalue: $\chi_1=3-\dfrac{3k_ck_r}{2k_s^2(\lambda+1)}$, eigenstate: $\mathbf{h}_1=\dfrac{1}{\sqrt{3}}[1;1;1]$, $|\sigma_1|=p$.
- One-dimensional subspace of pure shears:
  Eigenvalue: $\chi_2=\dfrac{k_ck_r}{2k_s^2}$, eigenstate: $\mathbf{h}_2=\dfrac{1}{\sqrt{2}}[1;0;-1]$, $|\sigma_2|=\tau_{\max}$.

- One-dimensional subspace of deviators:
  Eigenvalue: $\chi_3 = \dfrac{3k_c k_r(1-\lambda)}{2k_s^2(1+\lambda)}$, eigenstate: $\mathbf{h}_3 = \dfrac{1}{\sqrt{6}}[1;-2;1]$, $|\sigma_3| = \tau_{45}$.

Contribution of certain stress states can be analyzed now. The first eigenstate $\mathbf{h}_1$ corresponds to the hydrostatic stress. Since inequality $\sigma_1 \geq \sigma_2 \geq \sigma_3$ is assumed, one can see that the second eigenstate $\mathbf{h}_2$ corresponds to maximum shear stress – please note that the contribution of this stress state to the total measure of material effort is independent of the anisotropy coefficient λ. The third eigenstate $\mathbf{h}_3$ is a composition of two non-orthogonal pure shears (we are considering classical scalar product defined as $\mathbf{A}\cdot\mathbf{B} = A_{ij}B_{ij}$); however, it is not a pure shear itself. Eigenstate $\mathbf{h}_3$ is orthogonal to the maximum shear state $\mathbf{h}_2$, but none of its pure shear components is orthogonal to $\mathbf{h}_2$. Please note that the inequalities $\sigma_1 \geq \sigma_2 \geq \sigma_3$ refer to the stress state $\boldsymbol{\sigma}$ itself, not to the projections of $\boldsymbol{\sigma}$ on chosen states, so it does not matter that those inequalities are not fulfilled in case of $\mathbf{h}_3$. Decomposition of the general stress state in the basis of eigenstates of the limit state operator, can be illustrated as shown in Fig. 1.

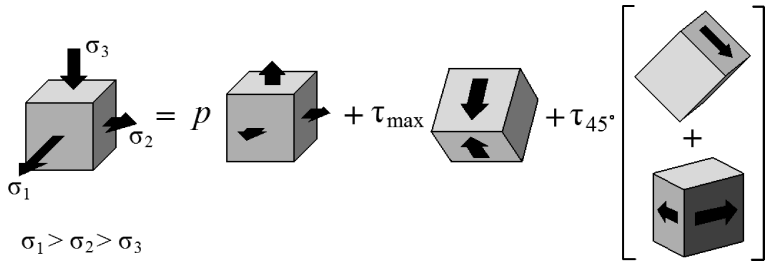

FIG. 1. Stress state decomposition in the basis of eigenstates of the limit state operator.

3. Critical review of the Burzyński criterion

In spite of its generality and clear physical interpretation in the sense of elastic energy, accompanied by mathematical simplicity, one has to note that Burzyński's limit criterion for anisotropic solids is not stated correctly in all of its aspects. General idea of an energy-based criterion with additional function defining contribution of volumetric strain in material effort, is of greatest importance and it emerges to be a simple and effective way to account for i.e. the strength-differential effect in other energy-based hypotheses (see R.B. Pęcherski *et al.* [8], J. Ostrowska–Maciejewska *et al.* [9]). However, there are few misstatements that were not pointed out and discussed in the literature; the main issues which have to be discussed are:

- Principal stress formulation.
- Lack of invariance of the parameters of the criterion.

- Basic coordinate system.
- Anisotropy coefficient λ.
- Isotropy of strength properties.
- Non-unique relation between elastic and strength parameters.

3.1. Principal stress formulation

Burzyński's criterion simplicity is in fact mainly due to its formulation in terms of principal stresses. Practical application of the limit condition (2.11) given by Burzyński (e.g. in numerical computations) enforces the use of the principal stresses directions coordinate system. One should notice that if the parameters of the criterion are to be constant (as it seems to be assumed by Burzyński), one has to assume that (due to anisotropy of the material and especially due to arbitrary orientation of the principal stresses) the whole formulation of the criterion should be invariant with respect to rotations and reflections; it would be isotropic then, what would be an obvious inconsistency. Otherwise, the value of those parameters must change depending on the chosen coordinate system – it is so in case of Burzyński's condition, however this problem was even not mentioned in [1]. It will be discussed in details in the next subsection.

Coordinate system built upon principal stresses directions is not holonomic – local coordinate system at a given point cannot be obtained through differentiation of a position vector along certain curves in the space at that point (especially when inequalities $\sigma_1 \geqslant \sigma_2 \geqslant \sigma_3$ have to be fulfilled), since the stress state distribution changes both in time and space and it may contain singularities or discontinuities.

Stress state determination requires exactly six parameters – six stress state components in any coordinate system or equivalently three stress tensor invariants or principal stresses, and three quantities describing the orientation of the principal stresses directions in the given coordinate system, i.e. three Euler angles or components of the versors indicating directions of principal stresses (nine components with six constraints – three orthogonality conditions and three normalization conditions). Referring only to three parameters, the principal values of the stress tensor does not give us full information about the stress state, which is especially important in case of anisotropic bodies. Simple example should make the problem clear – it is rather obvious that a certain stress state (set of eigenvalues) with its maximal component parallel to the wood fibers, cause much lower material effort than the same set of stresses applied in such a way that the maximal one is perpendicular to the fibers. In case of anisotropic materials, the values of the principal stresses alone are not a sufficient information for the description of the material effort, unless directions of the stresses are fixed. This

is also the reason for which any plot of the limit surface for anisotropic bodies in the space of principal stresses, refer in general only to a single, fixed orientation or principal stresses.

3.2. Lack of invariance of stiffness moduli

Stiffness parameters of an anisotropic body (used in criterion) depend strictly on the orientation of a sample referring to the given coordinate system, thus parameters of the criterion must change their values as a result of rotation of the coordinate system, since the directions of principal stresses (which are in fact arbitrary oriented) change – unless these parameters are invariants. It seems that Burzyński might tacitly assume that the parameters of his criterion are constant, which in his energy-based formulation could be possible only if they were invariants. Bulk modulus B as a quantity proportional to a Kelvin modulus of any volumetrically isotropic material is indeed an invariant. Yet all other stiffness moduli used in the criterion, namely L, M, N, which are defined (see relations (2.9)) as a difference between an invariant and a single component of $\mathbf{C}$ (which is not invariant due to anisotropy of $\mathbf{C}$), will in general change their values as the orientation of the coordinate system changes – thus even the name of '*generalized moduli of distortion*' is in fact not strictly correct. Because of lack of invariance of those parameters, whole formulation of the criterion given by Burzyński depends strongly on the choice of coordinate system, which always has to be the principal stresses directions coordinate system. Change of orientation of principal stresses may even cause not only quantitative but also qualitative modification of a yield surface at the given point – i.e. ellipsoidal (brittle materials, closed surface) into paraboloidal (hydrostatic pressure as a safe stress state).

The only solution which seems possible is to consider only the special class of stress states of fixed orientation of principal stresses directions. Yet such constraint is still not sufficient – even in case of coordinate system adapted to the directions of principal stresses and even if the orientation of stresses is fixed (due to e.g. specific use of the element made of the considered material or due to specific way of loading), the coordinate system should be chosen in such way that inequalities $\sigma_1 \geqslant \sigma_2 \geqslant \sigma_3$ will be satisfied. If the values of principal stresses change so that the discussed inequalities in the given coordinate system are no longer true, the coordinate system must be rotated by 90 degrees – in general such rotation is not an element of the symmetry group of arbitrarily chosen anisotropic material, even when volumetrical isotropy is assumed. Burzyński has written clearly that '*current and continued mathematical argument is in present conditions valid only with the assumption of inequality* $\sigma_1 \geqslant \sigma_2 \geqslant \sigma_3$, [1] – it can be easily shown that (using Burzyński's assump-

tions) the criterion is not fulfilled in case of uniaxial limit state when one takes: $(\sigma_1 = 0;\ \sigma_2 = k_r;\ \sigma_3 = 0)$. This was the way which (with assumption of equalities $\dfrac{M}{L} = \dfrac{M}{N} = 2(1-\lambda)$ which will be discussed below) allowed Burzyński to formulate the condition in such a way that it is indeed fulfilled in case of the limit uniaxial state, what (without those assumptions) is generally not true. Thus the coordinate system (and consistently parameters of the criterion which define the type of a yield surface) change as both orientation or value of principal stresses change.

Rejecting the necessity of fulfilling the system of inequalities $\sigma_1 \geqslant \sigma_2 \geqslant \sigma_3$ (or the inverse one) leads to conclusion that the limit stress in the direction of σ_2 is different than in the directions of two other principal stresses – Eq. (2.11) could be interpreted as a limit condition for the material with anisotropic strength properties for a set of stress states, with fixed principal stresses directions (i.e. parallel to the material symmetry axes). Assuming that k_{ri} and k_{ci} denote tensile and compression strength along the i-th axis respectively $(i = 1, 2, 3)$, one can find that neglecting inequalities $\sigma_1 \geqslant \sigma_2 \geqslant \sigma_3$, the limit condition (2.11) gives us:

$$
\begin{aligned}
&k_{r1} = k_{r3} = k_r, \qquad k_{c1} = k_{c3} = k_c, \qquad k_{s2} = \pm k_s,\\
&k_{c/r2} = \frac{-k_s^2(\lambda+1)(k_c - k_r)}{2(\lambda+1)k_s^2 + (1-2\lambda)k_c k_r}\\
&\qquad\qquad \pm \frac{k_s\sqrt{(\lambda^2+2\lambda+1)(k_c+k_r)^2k_s^2 - 2(2\lambda^2+\lambda-1)k_c^2k_r^2}}{2(\lambda+1)k_s^2 + (1-2\lambda)k_c k_r},\\
&k_{s1} = k_{s3} = \pm\sqrt{\frac{2(\lambda+1)}{5-4\lambda}}k_s,
\end{aligned}
\tag{3.1}
$$

what would be suitable for cylindrical or tetragonal symmetry – similar limit criterion for cylindrical symmetry formulated in terms of principal stresses, assuming that their directions are fixed, was analyzed by Theocaris [10]. The above purely mathematical considerations require the expressions under root to be positive. From the expression for $k_{s1} = k_{s3}$ we obtain $\lambda \in (-1; 1.25)$ – this is an interval of possible values of λ for which the above considerations have sense. Furthermore, we require that the term under the root in the formula expressing $k_{c/r2}$ is positive, what leads to the following inequality:

$$
\frac{(\lambda^2+2\lambda+1)}{(2\lambda^2+\lambda-1)} > \frac{2k_c^2k_r^2}{(k_c+k_r)^2k_s^2}. \tag{3.2}
$$

Physical interpretation of the obtained solutions requires also that the values of tensile and compression strength along x_2 must have different signs, $k_{c2}\cdot k_{r2} < 0$.

Here is a slight inconsistency in the notation in this case, since Burzyński has always considered both k_c and k_r to be positive. However, it does not influence the solution – using well-known Viète's formulas for the product of the roots of the polynomial, we obtain:

$$\frac{(2\lambda - 1)}{(\lambda + 1)} < \frac{2k_s^2}{k_c k_r}. \tag{3.3}$$

However, it has to be emphasized that in the general case, distinguishing of the intermediate stress in Burzyński's formulation must not be mistaken with distinguishing of a certain direction in the material (i.e. as in transversal isotropy), as sometimes it is understood. If a symmetry of the material is described in a given coordinate system ($\mathbf{e}_1$, $\mathbf{e}_2$, $\mathbf{e}_3$) and directions of the principal stresses are determined by a set of versors ($\mathbf{e}'_1$, $\mathbf{e}'_2$, $\mathbf{e}'_3$) which in general do not correspond with the given coordinate system, then special meaning of intermediate stress is the distinction of $\mathbf{e}'_2 \otimes \mathbf{e}'_2$ (or at most $\mathbf{e}'_2$) having nothing to do with independent of the stress state (thus constant at all points) direction in physical space given by $\mathbf{e}_2$.

3.3. Basic coordinate system

Another inconsistency which has to be discussed is the existence of the basic coordinate system given by a set of equalities (2.7). Its physical interpretation is not quite clear. It is obvious that the coordinate system of principal stresses directions (as well as the one of principal directions of the strain state which in case of anisotropy is not always coaxial with stress state – furthermore, Rychlewski has shown that there exists no such an anisotropic linear elastic material which preserves the coaxiality of stress and strain tensors [11]) is such basic coordinate system – yet it depends on the stress or strain state and thus it is different at each point, what makes it rather impractical in use. Also in case of orthotropy and any other higher symmetry, such basic coordinate system actually exists – axes of such system are parallel to the axes of symmetry of the considered material. Both such systems can be set using simple rotation in physical space, so it is not *'only mathematically possible'*.

However, it is not quite clear if the basic coordinate system really exists in case of lower symmetries (total anisotropy, monoclinic symmetry, trigonal symmetry) independently of the form of stress state – or, speaking in other way, whether there exists such orientation of a coordinate system in physical space, being characteristic for the material (not only for the stress state as in case of principal stresses), which makes it the basic one. There are *'mathematically possible'* rotations in six-dimensional space of symmetric second-order tensors which do not refer to any rotation in physical space, thus there might be no such

a real rotation which would satisfy conditions (2.7) for any values of the stress state components. If so, then referring to the compliance tensor components in the relations (2.7) is unnecessary, since the basic coordinate system would be only a stress state-dependent. Actually, even defining such specific coordinate system with the relations (2.7) would be senseless since one always has to take a local coordinate system built upon directions of the principal stresses. Furthermore, if there exists no such a rotation in physical space which would give us the basic coordinate system, then the coordinate system transformation given by (2.7) changes the physical meaning of the components of both the compliance and stress tensor – e.g. components of the stress tensor (appearing in energy density formulation) may emerge to be of an abstract nature - they could not be interpreted as normal or shear stresses. The simplification of the elastic energy density formulation presented by Burzyński might emerge not as general as it first seemed to be and it should be constrained either to the systems of principal stresses direction or one should consider only orthotropy or higher symmetry.

Finding the solution of the problem of existence of the basic coordinate system is equivalent to answering the question if there exists such a basis in physical space in which any compliance tensor $\mathbf{C}$ of a volumetrically isotropic material takes the following form:

$$\mathbf{C} \cong \begin{bmatrix} C_{1111} & C_{1122} & C_{1133} & 0 & 0 & 0 \\ & C_{2222} & C_{2233} & 0 & 0 & 0 \\ & & C_{3333} & 0 & 0 & 0 \\ & & & C_{2323} & C_{2331} & C_{2312} \\ & \text{sym} & & & C_{3131} & C_{3112} \\ & & & & & C_{1212} \end{bmatrix}. \tag{3.4}$$

For this very general analysis it is enough to notice that the number of independent components of the compliance tensor of arbitrary symmetry is further decreased from 16 to 10 (please note that the Burzyński's conditions (2.4) still have to be fulfilled) – this indicates that there exist volumetrically isotropic compliance tensors for which there is no such orientation in the physical space, which makes the coordinate system the basic one.

3.4. Anisotropy coefficient λ

As it was shown above in Eq. (2.11), the anisotropy of elastic properties of the considered material was represented by a single parameter λ. It was defined as $\lambda = \dfrac{M^2}{2LN}$. It was also assumed by Burzyński that $\dfrac{M}{L} = \dfrac{M}{N} =$

$2(1-\lambda)$, which is an additional constraint for possible values of parameter λ. It is a consequence of a specific form of the criterion formulation – it can be shown that only if these equalities are true, the criterion is fulfilled in limit uniaxial stress states. Burzyński did not discuss these constraints and stated only that '*it seems reasonable to expect that the interval within which* λ *varies is quite modest, and so that it ranges e.g. from 0 to 1*' [1]. Putting $x = \dfrac{M}{L} = \dfrac{M}{N}$ we obtain $\lambda = \dfrac{M^2}{2LN} = \dfrac{1}{2}x^2$ and finally, substituting both relations in $\dfrac{M}{L} = \dfrac{M}{N} = 2(1-\lambda)$, we obtain the following equation:

$$x^2 + x - 2 = 0. \tag{3.5}$$

There are two roots of the above equation $x_1 = -2$ and $x_2 = 1$. The first one has to be rejected because x was defined as a fraction of two '*stiffness moduli*', which are assumed to be positive. Thus the only result is $x = 1$ which gives us $\lambda = \dfrac{1}{2}$, the value of λ for which the criterion is identical as the criterion for isotropic bodies.

It has to be mentioned that before giving the simplified form of the proposed limit condition (2.11), Burzyński wrote: "[parameters M/N, M/L, M^2/LN] *are not treated* [now] *as representations of the ratio of elasticity constants, but as coefficients particularly connected with the experimental essence of material effort*" [1]. It is not clear how to interpret these words – assuming that in this short sentence Burzyński rejected all previous assumptions on λ (see relations (2.10)), makes all further derivations deprived of theoretical foundation and physical, energy-based interpretation as long as $\lambda \neq \dfrac{1}{2}$. One should remember also that the limit criterion introduced by Burzyński, depends on 4 independent parameters and simple strength tests give us only three values of which the criterion parameters are dependent. Some parameters (e.g anisotropy coefficient λ) must also take into consideration any information about the elastic structure of the material, so they cannot be "*connected*" o n l y "*with the experimental essence of material effort*" – unless there exists a one-to-one correlation between elastic and strength properties of the considered body. This problem is discussed in Subsec. 3.6.

3.5. Isotropy of strength properties

Finally one should also notice that in the whole paper by Burzyński [1] there is no such thing mentioned as anisotropy of *strength properties*. Limit stresses k_c, k_r and k_s are assumed to be independent of the direction of loading.

This makes the criterion to some extent useless since it assumes that each (tensile, compression, shearing) limit stress is the same in any direction, despite the anisotropy of elastic properties of the body.

3.6. Non-unique relation between elastic and strength parameters

Widely known failure criteria formulated by HILL [5] and HOFFMAN [6] are influenced by their parameters in a linear way. In any such criterion under certain conditions, those parameters can be uniquely expressed in terms of limit stresses. Yield surface can be determined basing only on simple strength tests: uniaxial tension and compression and pure shears in three perpendicular directions. However, the parameters of both mentioned criteria were not interpreted in a strictly physical way. In the contrary to them, most of parameters of Burzyński's criterion (except ω, δ and K) have precise physical meaning and their values can be either directly measured or, at least, estimated through performance of a series of tests and analysis of the obtained elastic constants. They influence the criterion in a linear way, so there might exist one-to-one correlation between them and limit values of stresses. If such relation existed, those parameters could be determined in two ways – by direct measurements of the elastic properties of the body or in a series of simple strength tests. This would indicate that elastic properties of the material determine uniquely its strength properties. Authenticity of such statement should be verified experimentally, however it seems that there might exist two materials of different internal structure, which exhibit macroscopically the same elastic properties but different strength properties (e.g. due to different mechanisms of yielding).

Let us return to the basic form of the failure condition, rejecting later substitutions made by Burzyński. For further simplification, let us assume the we are not considering the cases of symmetries lower than ortothropy, so there exists a fixed coordinate system, independent of the stress state, in which at every point the elastic energy density can be expressed in the form given by Eq. (2.8). Simply substituting (2.8) into (2.2), we obtain:

$$\begin{aligned}(3.6)\qquad &\frac{1}{2}B_\omega(\sigma_{11}+\sigma_{22}+\sigma_{33})^2+\frac{1}{2}B_\delta(\sigma_{11}+\sigma_{22}+\sigma_{33})\\ &\qquad+\frac{1}{3}\left[L(\sigma_{22}-\sigma_{33})^2+M(\sigma_{33}-\sigma_{11})^2+N(\sigma_{11}-\sigma_{22})^2\right]\\ &\qquad+2P\sigma_{23}^2+2Q\sigma_{31}^2+2R\sigma_{12}^2-K=0,\end{aligned}$$

where $B_\omega = B\omega$, $B_\delta = B\delta$. One can note that if the condition (3.6) is fulfilled for certain values of its parameters, it is also fulfilled if all of them are multiplied by the same constant – this indicates that the relation between those

parameters and limit stresses obtained from strength tests cannot be unique. Let us divide (3.6) by K so that we obtain the limit conditions depending on five parameters:

$$\begin{aligned}(3.7)\qquad &\frac{1}{2}\widetilde{B_\omega}(\sigma_{11}+\sigma_{22}+\sigma_{33})^2+\frac{1}{2}\widetilde{B_\delta}(\sigma_{11}+\sigma_{22}+\sigma_{33})\\ &+\frac{1}{3}\left[\widetilde{L}(\sigma_{22}-\sigma_{33})^2+\widetilde{M}(\sigma_{33}-\sigma_{11})^2+\widetilde{N}(\sigma_{11}-\sigma_{22})^2\right]\\ &+2\widetilde{P}\sigma_{23}^2+2\widetilde{Q}\sigma_{31}^2+2\widetilde{R}\sigma_{12}^2=-1,\end{aligned}$$

where the parameters with tilde denote the corresponding parameters from (3.6) divided by K.

Assuming pure shear tests, one can easily find

$$\widetilde{P}=\frac{1}{2k_{s1}^2},\qquad \widetilde{Q}=\frac{1}{2k_{s2}^2},\qquad \widetilde{R}=\frac{1}{2k_{s3}^2}.$$

Let us assume that strength properties of the considered body are anisotropic and also that in every direction it exhibits the strength-differential effect. In such case, condition (3.6) has to be fulfilled in six uniaxial states which gives us following overdetermined system of six equations for five parameters of the criterion (contrary to the notation used by Burzyński we assume $k_r>0$, $k_c<0$):

$$(3.8)\qquad \frac{1}{3}\begin{bmatrix} 0 & k_{r1}^2 & k_{r1}^2 & \frac{3}{2}k_{r1} & \frac{3}{2}k_{r1}^2\\ k_{r2}^2 & 0 & k_{r2}^2 & \frac{3}{2}k_{r2} & \frac{3}{2}k_{r2}^2\\ k_{r3}^2 & k_{r3}^2 & 0 & \frac{3}{2}k_{r3} & \frac{3}{2}k_{r3}^2\\ 0 & k_{c1}^2 & k_{c1}^2 & \frac{3}{2}k_{c1} & \frac{3}{2}k_{c1}^2\\ k_{c2}^2 & 0 & k_{c2}^2 & \frac{3}{2}k_{c2} & \frac{3}{2}k_{c2}^2\\ k_{c3}^2 & k_{c3}^2 & 0 & \frac{3}{2}k_{c3} & \frac{3}{2}k_{c3}^2 \end{bmatrix}\begin{bmatrix}\widetilde{L}\\ \widetilde{M}\\ \widetilde{N}\\ \widetilde{B}_\delta\\ \widetilde{B}_\omega\end{bmatrix}=\begin{bmatrix}1\\1\\1\\1\\1\\1\end{bmatrix}.$$

One can observe that the fifth column of the matrix of coefficients, the one corresponding to the $\widetilde{B}_\omega$ parameter (quadratic pressure influence), can be expressed as a linear combination of the first three columns corresponding to shear moduli $\widetilde{L}$, $\widetilde{M}$, $\widetilde{N}$ – both of two possible 5×5 minors must be then equal to 0 what indicates that the rank of the matrix of coefficients is equal at most to 4. The rank of the augmented matrix is equal to 5, thus it is an inconsistent system of equations and no solution can be found.

4. Proposition of different formulation of the limit criterion

It seems to the author that the final form of the limit condition should depend on Burzyński's stiffness moduli in their unchanged form (their values can be well estimated) and only the parameters K, δ, ω should be determined in a numerical way so that the obtained limit surface fitted the experimental data well. This would give us only three independent parameters which could be used to fit the model to nine independent strength tests. Despite the fact that K, δ, ω are independent of the elastic constants, it is clear that elastic properties would influence the measure of material effort very strongly. Good correlation between the determined model and the experimental results would verify the correctness of Burzyński's hypothesis, in particular the form of the influence function assumed by him. Having determined the limit condition for a sufficiently large set of materials of similar class, may enable finding empirical formulas for the unknown parameters, e.g. $K = K(B, L, M, N, \ldots, k_{r1}, k_{r2}, \ldots, k_{s3})$. In the further analysis, the found formulas for different classes of materials could be compared.

Yet, assuming that parameters K, ω, δ are known as well as the elastic moduli B, L, M, N, P, Q, R, limit stresses can be easily found from the system of Eq. (3.8).

$$
\begin{aligned}
k_{c/r1} &= \frac{-3\widetilde{B}_\delta \pm \sqrt{16(\widetilde{N}+\widetilde{M})+24\widetilde{B}_\omega+9\widetilde{B}_\delta^2}}{4(\widetilde{N}+\widetilde{M})+6\widetilde{B}_\omega},\\
k_{c/r2} &= \frac{-3\widetilde{B}_\delta \pm \sqrt{16(\widetilde{N}+\widetilde{L})+24\widetilde{B}_\omega+9\widetilde{B}_\delta^2}}{4(\widetilde{N}+\widetilde{L})+6\widetilde{B}_\omega},\\
k_{c/r3} &= \frac{-3\widetilde{B}_\delta \pm \sqrt{16(\widetilde{M}+\widetilde{L})+24\widetilde{B}_\omega+9\widetilde{B}_\delta^2}}{4(\widetilde{M}+\widetilde{L})+6\widetilde{B}_\omega},
\end{aligned}
\tag{4.1}
$$

$$
\begin{aligned}
k_{s1} &= \sqrt{\frac{K}{2P}},\\
k_{s2} &= \sqrt{\frac{K}{2Q}},\\
k_{s3} &= \sqrt{\frac{K}{2R}}.
\end{aligned}
$$

The set of acceptable values of parameters K, ω, δ is determined by the following system of inequalities, which are required for the existence of two real solutions k_{ci}, k_{ri} of different signs:

$$
\begin{aligned}
16(N+M)+24B\omega+9(B\delta)^2>0,\\
16(N+L)+24B\omega+9(B\delta)^2>0,\\
16(L+M)+24B\omega+9(B\delta)^2>0,\\
N+M+\frac{3}{2}B\omega>0,\\
N+L+\frac{3}{2}B\omega>0,\\
L+M+\frac{3}{2}B\omega>0.
\end{aligned}
\tag{4.2}
$$

First three inequalities guarantee positiveness of the expressions under the roots what leads to $k_{ci}, k_{ri} \in \mathbb{R}$ and $k_{ci} \neq k_{ri}$ and last three inequalities are derived using Viète's formulas from the condition $k_{ci} \cdot k_{ri} < 0$ $(i = 1, 2, 3)$. Please note that further constraints for the range of acceptable values of the parameters K, ω, δ can be assumed – e.g. condition of convexity of the limit surface.

5. Summary

It has been shown that failure condition formulation given by Burzyński based on his hypothesis of material effort is not stated correctly in various aspects. However, his original proposition of a hypothesis is of greatest scientific value. It is only the final condition that has to be reformulated. As a concluding remark, it is worth noting that hypothesis of Burzyński distinguishes itself among other similar propositions with certain advantages – it is stated in terms of quantities of clear physical meaning and it enables using large variety of limit surfaces for the description of the limit states for different classes of materials. Great effort made by Burzyński to express the limit condition using possibly small number of parameters, was to make the hypothesis easily applicable in computation; unfortunately it led him to a series of misstatements. However, those inconsistencies do not diminish great importance of the general idea of Burzyński – measure of material effort considered as a combination of independent energy densities, which contribution is determined by a proper stress state – dependent function.

References

1. W. Burzyński, *Studium nad hipotezami wytężenia*, Akademia Nauk Technicznych, Lwów 1928; see also: *Selected passages from Włodzimierz Burzyński's doctoral dissertation "Study on material effort hypotheses"*, Eng. Trans., **57**, 3–4, 185–215, 2009.
2. M. T. Huber, *Właściwa praca odkształcenia jako miara wytężenia materyału*, Czasopismo Techniczne, **15**, Lwów, 1904; see also: *Specific work of strain as a measure of material effort*, Arch. Mech., **56**, 3, 173–190, 2004.
3. D. C. Drucker, W. Prager, *Soil mechanics and plastic analysis for limit design*, Quart Appl. Mat., **10**, 2, 157-–165, 1952.
4. R. von Mises, *Mechanik der plastischen Formanderung von Kristallen*, Zeitschrift für Angewandte Methematik und Mechanik, **8**, 161–185, 1928.
5. R. Hill, *A theory of the yielding and plastic flow of anisotropic metals*, Proc. Roy Soc. London, **193**, 281–297, 1948.
6. O. Hoffman, *The brittle strength of orthotropic materials*, J. Comp. Mater., **1**, 200–206, 1967.
7. K. Kowalczyk–Gajewska, J. Ostrowska–Maciejewska, *The influence of internal restrictions on the elastic properties of anisotropic materials*, Arch. Mech., **56**, 3, 205–232, 2004.
8. R. B. Pęcherski, P. Szeptyński, M. Nowak, *An extension of Burzyński hypothesis of material effort accounting for the third invariant of stress tensor*, Arch. Metall. Mat., **56**, 2, 503–508, 2011.
9. J. Ostrowska–Maciejewska, R. B. Pęcherski, P. Szeptyński, *Limit condition for anisotropic materials with asymmetric elastic range*, Engng. Trans. – submitted for publication.
10. P. S. Theocaris, *Failure criteria for transtropic, pressure dependent materials*, Rheol. Acta, **27**, 451–465, 1988.
11. J. Rychlewski, *A qualitative approach to Hooke's tensors. Part II*, Arch. Mech., **53**, 1, 45–63, 2001.

Received April 6, 2011; revised version June 28, 2011.